Available online at www.sciencedirect.com

SciVerse ScienceDirect

Geochimica et Cosmochimica Acta 110 (2013) 253–273

Geochimica et Cosmochimica Acta

www.elsevier.com/locate/gca

Dissolved organic carbon dynamics in anaerobic sediments of the Santa Monica Basin

Tomoko Komada [a,*], David J. Burdige [b], Sabrina M. Crispo [a,1], Ellen R.M. Druffel [c], Sheila Griffin [c], Leah Johnson [a,2], Diemmi Le [a]

[a] Romberg Tiburon Center, San Francisco State University, Tiburon, CA 94920, United States
[b] Department of Ocean, Earth and Atmospheric Sciences, Old Dominion University, Norfolk, VA 23529, United States
[c] Department of Earth System Science, University of California Irvine, Irvine, CA 92607-1300, United States

Received 23 May 2012; accepted in revised form 11 February 2013; Available online 27 February 2013

Abstract

Cycling of dissolved organic carbon (DOC) was investigated in anoxic sediments of the Santa Monica Basin, California Borderland, by analyzing the concentration and isotopic signatures ($\Delta^{14}C$ and $\delta^{13}C$) of pore-water DOC and dissolved inorganic carbon (DIC), and organic compound classes extracted from the bulk sediments. DOC and DIC increased across the sediment–water interface, indicating net efflux of these solutes out of the sediments. Throughout the depth interval examined (0–30 cm), the $\Delta^{14}C$ value of DOC ($\Delta^{14}C_{DOC}$) was similar to, or higher than, that of bulk sedimentary particulate organic carbon (POC), indicating degradation of relatively ^{14}C-rich components of POC. There were prominent peaks in both $\Delta^{14}C_{DOC}$ and $\Delta^{14}C_{DIC}$ in the uppermost 2 cm of the sediment column, indicating degradation and remineralization of ^{14}C-rich, labile organic matter in the near-surface sediments. However, below these sub-surface maxima, $\Delta^{14}C_{DOC}$ and $\Delta^{14}C_{DIC}$ decreased with depth by ~200‰ and ~50‰, respectively. Given the diffusive time scales, these decreases were too large to be explained by ^{14}C loss due to radioactive decay. To help explain these observations, we constructed and implemented a selective degradation model that considers bulk pore-water DOC to be the sum of three kinetically- and isotopically-distinct sub-components. Based on this model, the most reactive DOC fraction, which supported ~60% of the DIC production, had a $\Delta^{14}C$ value indicating the presence of bomb-^{14}C. The intermediate fraction had a $\Delta^{14}C$ value of ~−60‰ and accounted for most of the pore-water DOC standing stock. The least reactive fraction was virtually non-reactive in these sediments, and had a $\Delta^{14}C$ value of ~−500‰. The benthic DOC flux of this ^{14}C-depleted, poorly-reactive DOC fraction may represent a source of pre-aged, refractory DOC to the oceans.

1. INTRODUCTION

Continental margin sediments play a key role in the marine and global cycles of carbon through active organic matter degradation and burial (Hedges and Keil, 1995; Burdige, 2007). While particulate organic carbon (POC) undergoing degradation is mostly remineralized to dissolved inorganic carbon (DIC) and inorganic nutrients, it has been found that <~10% of POC undergoing degradation accumulates as dissolved organic carbon (DOC) in the pore waters (Alperin et al., 1999; Burdige, 2002; Fig. 1). This net DOC production in turn supports an efflux of DOC out of the sediments to the water column. Globally, marine sediments are estimated to supply DOC to the water column at a rate comparable to global riverine DOC fluxes (~0.18 Gt yr^{-1}; Burdige et al., 1999). Despite this quantitative importance, the significance of net DOC production in the marine carbon cycle remains unclear, because of a lack

* Corresponding author. Tel.: +1 415 338 3748; fax: +1 415 435 7120.
E-mail address: tkomada@sfsu.edu (T. Komada).
[1] Present addresses: Environmental Chemistry Laboratory, California Department of Toxic Substances Control, Berkeley, CA 94710, United States. Sequoia Foundation, 2166 Avenida De La Playa Ste F, La Jolla CA 92037 United States.
[2] Present address: School of Oceanography, University of Washington, Seattle, WA 98195, United States.

0016-7037/$ - see front matter © 2013 Elsevier Ltd. All rights reserved.
http://dx.doi.org/10.1016/j.gca.2013.02.017

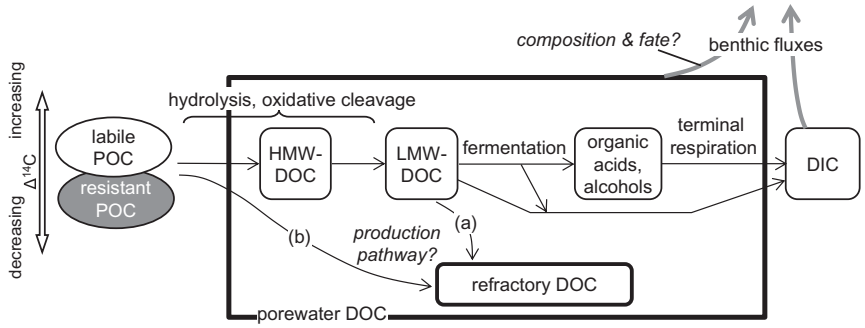

Fig. 1. Organic carbon degradation in sulfate-reducing sediments (see e.g., Fenchel et al. (1998) and Arnosti (2010) for further details). POC is first converted into high-molecular-weight DOC (HMW-DOC) via hydrolysis and/or oxidative cleavage. HMW-DOC is further transformed into low-molecular-weight (LMW) DOC, such as amino acids and monosaccharides. Fermentation converts LMW-DOC into short-chain organic acids and alcohols (along with CO_2 and H_2), which are respired to DIC. Sulfate reducers can also directly oxidize some LMW-DOC to DIC. Two possible pathways for the formation of refractory DOC are shown: (a) internal conversion of originally-labile HMW- or LMW-DOC (Burdige and Gardner, 1998), (b) direct production from POC solubilization (Robador et al., 2010; Komada et al., 2012). Benthic DOC fluxes are supported by a mixture of labile and refractory porewater DOC. $\Delta^{14}C$ signatures were used in this study as proxy for OC reactivity (far left of the figure; see text for details).

of understanding of the mechanism for DOC production, and the composition and reactivity of DOC that accumulates in the pore waters.

Pore-water DOC composition has been investigated through quantification of specific compounds (e.g., short-chain organic acids, amino acids; Sansone and Martens, 1982; Burdige and Martens, 1990) and major classes of biomolecules (Lomstein et al., 1998; Burdige et al., 2000). These studies show that such identifiable components can be relatively abundant near the sediment–water interface, but overall are a minor fraction of the pore-water DOC pool due to their high reactivity. The majority of pore-water DOC instead consists of moieties that are not readily characterized by conventional analytical techniques (Burdige, 2001, 2002). This apparent structural complexity of pore-water DOC is consistent with findings from ultra-high-resolution mass spectrometry (Koch et al., 2005; Tremblay et al., 2007; Schmidt et al., 2011). Investigation into the molecular size distribution of pore-water DOC further shows that with the exception of near-surface sediments where high-molecular-weight (>1 kDa) DOC is relatively abundant, pore-water DOC is dominated by components of lower molecular weight (Burdige and Gardner, 1998). This has led to the hypothesis that analogous to DOC in the water column (Amon and Benner, 1996), most pore-water DOC consists of highly degraded, low-molecular-weight material of limited reactivity (Burdige and Gardner, 1998). The presence of poorly-reactive DOC in sediment pore waters has been supported by laboratory incubation experiments (Hee et al., 2001; Komada et al., 2012), and through modeling studies (Burdige, 2002; Komada et al., 2004).

The occurrence of DOC that resists degradation in the pore waters leads to two major questions (Fig. 1). First, how is refractory DOC produced in sediments, and how is its production related to the overall degradation and remineralization of organic carbon (OC) in the sediments? There are two standing hypotheses for the origin of recalcitrant DOC in sediments: production within the pore waters themselves through alteration of originally labile monomers (pore water size reactivity model; Burdige and Gardner, 1998), and production of refractory DOC directly from POC hydrolysis (Robador et al., 2010; Komada et al., 2012). Second, what is the composition of DOC that is exported to the water column, and what is the fate of this material in the water column? Modeling studies show that the benthic flux is dominated by labile, high-molecular-weight DOC whose production rate is high near the sediment–water interface (Burdige, 2001, 2002). This suggestion is consistent with high $\Delta^{14}C$ values reported for pore-water DOC collected from the surface sediments (0–10 cm depth) of the Santa Monica Basin, California Borderland, and Station N, located on the continental rise of the eastern North Pacific Ocean (Bauer et al., 1995). However, benthic DOC fluxes must also be supported at least in part by refractory DOC (Fig. 1). The significance of benthic DOC fluxes in the marine carbon cycle would depend strongly on the magnitude of this refractory DOC flux, and the reactivity of this material in the oxic water column (Alperin et al., 1999).

The goal of this study was to further investigate the mechanism of pore-water DOC accumulation, and to better understand the role of pore-water DOC in the overall organic matter degradation process. To achieve these goals, we determined ^{14}C and ^{13}C signatures of pore-water DOC and DIC in the suboxic to anoxic sediments of the Santa Monica Basin (SMB), California Borderland, and analyzed them using a selective degradation model. The ^{14}C signatures were used as proxies for OC reactivity, where high ^{14}C abundance (high $\Delta^{14}C$, young radiocarbon age) was interpreted to indicate the presence of young, reactive material, and low ^{14}C abundance (low $\Delta^{14}C$, old radiocarbon age) was interpreted to indicate the presence of aged material of limited reactivity (e.g., Trumbore, 2000; Mayorga et al., 2005; Repeta and Aluwihare, 2006; Blair and Aller, 2012; Fig. 1). As shown below, results obtained applying our selective degradation model to the pore water data support these assumptions. Finally, in addition to pore water constituents, we applied ^{14}C and ^{13}C measurements to

POC at the bulk and compound-class levels to help evaluate the components of POC undergoing hydrolysis and oxidation.

2. METHODS

2.1. Study site and sampling

Sediment cores were collected from the SMB, an inner basin of the California Borderland with a maximum water depth of 910 m, and sill depth of 725 m (Gorsline, 1992). The sediments of the basin floor are laminated (Christensen et al., 1994) due to low dissolved oxygen in the bottom waters (<10 μmol kg^{-1} O_2) which severely limits the population of benthic macrofauna. Bottom-water dissolved oxygen concentration at the time of sampling was ~2 μmol kg^{-1}. Major sources of sediment to SMB are the Ventura and Santa Clara rivers that discharge to the north of the basin (Gorsline et al., 2000). In addition to vertical particle flux from the surface waters, sediment delivery to the basin floor occurs by lateral transport of suspended fine particles (Huh et al., 1990), as well as in the form of seismically triggered sandy turbidites (Gorsline, 1996; Gorsline et al., 2000). The turbidites vary in magnitude and frequency, from thin (~5 cm thick) sections with a recurrence interval on the order of decades to a century (Gorsline, 1996; Gorsline et al., 2000), to >1 m thick deposits triggered by large events with a recurrence interval of 300–360 yrs (Romans et al. 2009). In between these turbidites are fine-grained deposits characteristic of hemipelagic sedimentation. The sedimentation rate for these layers appears to have remained steady over the last ~7000 yrs (Romans et al., 2009).

Sediment cores were recovered from the center of the SMB using a multicorer aboard the *R/V* Point Sur in July 2008 (33.749°N, 118.833°W, 900 m water depth). Cores were immediately transferred to a refrigerated van and processed within 2–9 h of recovery. Bottom-water DIC and DOC samples were collected with a Go Flo bottle following DOE (1994) and Beaupré et al. (2007), respectively. In the refrigerated van, sediment cores were extruded in an N_2 atmosphere at intervals of 0.25, 0.5, or 1.0 cm, to a depth of 45 cm. Sediment aliquots were centrifuged in polycarbonate tubes at 4 °C, and the supernatant was collected into all-polypropylene syringes with stainless steel needles, and filtered through disposable 0.2 μm Nylon filters with 0.7 μm GF/F pre-filter (Whatman 6870-2502). The first 3 mL were discarded. To minimize the DOC blank, 100 mL of UV-irradiated deionized water were pushed through each disposable filter prior to use. DIC samples for ^{13}C and ^{14}C abundances were immediately flame-sealed under a stream of ultra-high-purity (UHP) N_2 into 10–15 mL borosilicate tubes spiked with $HgCl_2$ (McCorkle et al., 1985). DOC samples were either acidified and ampoulated under a stream of UHP N_2 gas and refrigerated (cores 7–2 and 9–1), or frozen without acidification in 20 mL scintillation vials with Teflon-lined caps (all other cores). Frozen samples formed precipitates during storage, while refrigerated samples did not. Centrifuge tubes containing sediment were frozen. All tools and parts were first cleaned with household dish soap, then acid rinsed (exclusive of metal parts). Plasticware was air dried; glassware and metal tools were baked at 550 °C for 4 h.

2.2. Analytical methods

DOC concentrations were determined by high temperature combustion (HTC) using a Shimadzu TOC-V. For depth intervals where more than 1 vial or ampule was available, data from each container are reported. Frozen DOC samples were subsampled (while swirling to collect a representative split consisting of solution and precipitate), and diluted manually by mass to <120 μM prior to analysis. Two to four DOM consensus reference materials (Hansell laboratory, RSMAS) were analyzed each analytical day. LCW and DSR (batch# 07-08) concentrations averaged 0 ± 1 μM ($n = 30$) and 43 ± 1 μM ($n = 30$), respectively, which were close to the reported consensus values for these standards (1 μM and 41–44 μM, respectively).

A subset of frozen DOC samples was further processed for ^{14}C and ^{13}C by UV oxidation (UV_{ox}; Beaupré et al., 2007), and by thermal sulfate reduction (TSR; Johnson and Komada, 2011). Samples from core 6–7 were processed by UV_{ox} at UC Irvine; selected samples from cores 6–7, 8–7, and 10–8 were processed by TSR at SFSU. For both of these analyses, the entire contents of the vial, consisting of solution and precipitate, were processed to ensure quantitative recovery of DOC (Johnson and Komada, 2011). To account for any ^{14}C contamination that may have occurred during pore water collection, aqueous solutions of SRM 4990B and IAEA-C7 with concentrations similar to those of pore-water DOC were prepared in the laboratory, and variable volumes of these solutions were processed similarly to pore water samples (aspirated into all-propylene syringes, then filtered), and oxidized by UV_{ox}. The $\Delta^{14}C$ values of SRM 4990B ($n = 5$) and IAEA-C7 ($n = 6$) fell within ±19‰ and ±15‰ of the consensus values, respectively (Table 1).

Pore-water DIC samples were extracted by cracking the ampoules open under vacuum in the presence of 3 mL of 3 M H_3PO_4 saturated with $CuSO_4$ (McCorkle et al., 1985; Aller and Blair, 2006). The evolved CO_2 was dried, quantified to determine DIC concentration, and split into borosilicate breakseal tubes for determination of ^{13}C (0.1 mg C sample size) and for ^{14}C (0.1–1.2 mg C sample size). Bottom-water DIC for ^{13}C and ^{14}C measurements was extracted according to McNichol et al. (1994), quantified, and split for ^{13}C and ^{14}C measurements as described above. Bottom-water DIC concentration was also determined from a separate sample using a Monterey Bay Research Institute-clone DIC analyzer (Waltz and Friederich, 1996). DIC concentrations from the two analyses agreed to within 30 μM.

For determination of bulk POC, sediment was dried and powdered, fumigated with HCl to remove carbonates (Komada et al., 2008), and analyzed using a Costech ECS-4010. Total N was determined on non-fumigated samples. To determine ^{13}C and ^{14}C composition of POC, fumigated sediment was combusted in sealed quartz tubes at 850 °C for 4 h in the presence of CuO wire and Ag foil

Table 1
$\Delta^{14}C$ values of radiocarbon standards obtained by UV_{ox}. These standards were filtered and preserved in the same manner as the unknowns prior to UV oxidation (see text).

UCID[a]	Size (μg C)[b]	$\Delta^{14}C$ (‰)	Error (‰)[c]	Offset (‰)[d]
SRM 4990B (consensus value + 33‰)[e]				
12652	31	+34	±15	+1
12721	31	+52	±52	+19
12653	35	+20	±43	−13
12417	143	+23	±20	−10
12453	529	+35	±5	+2
IAEA-C7 (consensus value − 508‰)[e]				
12809	29	−515	±34	−7
12648	33	−514	±30	−6
12651	123	−507	±15	+1
12455	139	−523	±13	−15
12650	459	−513	±4	−5
12517	456	−496	±4	+14

[a] Internal identification numbers.
[b] Total amount of carbon present in each aliquot.
[c] Uncertainties reported by the UCI Keck Carbon Cycle AMS Laboratory.
[d] Deviation from the consensus value.
[e] Consensus values decay corrected to the year of analysis (2010).

(Druffel et al., 1992). The evolved CO_2 was cryogenically purified, quantified, and split as described above. POC compound classes were extracted from powdered sediment for isotopic analyses according to Wang et al. (1998). Briefly, total extractable lipids (TL) were first recovered by sonicating ~1 mg of sediment in 2:1 (v/v) methylene chloride–methanol (Fisher GC Resolv®). The acid-soluble (AS) fraction was extracted by hydrolyzing the solvent-extracted solids with 6 M HCl (J.T. Baker Instra-Analyzed®) at 100 °C for 19 h in an N_2 atmosphere. The non-hydrolysable residue was collected as the acid insoluble (AI) fraction. The TL fraction was blown down to dryness, acidified with H_3PO_4 (Fisher HPLC) and combusted as described above for bulk POC. The AI fraction was dried and combusted as described above for bulk POC. All AS fractions were lost during combustion due to quartz tube failure, hence the amount and isotopic composition of this fraction were calculated by mass balance (see Section 3.2).

CO_2 splits for ^{14}C determination were graphitized using a sealed tube zinc reduction method (Xu et al., 2007), and submitted to the Keck Carbon Cycle AMS Laboratory at UC Irvine for analysis by accelerator mass spectrometry (AMS). CO_2 splits for ^{13}C determination were submitted to the Stable Isotope Laboratory at UC Davis for analysis by dual-inlet isotope ratio mass spectrometry. ^{13}C abundances are reported using the δ notation (‰ deviation of the $^{13}C/^{12}C$ ratio relative to the standard V-PDB). ^{14}C abundances are reported using the $\Delta^{14}C$ notation (‰ deviation of the $^{14}C/^{12}C$ ratio relative to a 19th century wood standard normalized to $\delta^{13}C$ of −25‰; Stuiver and Polach, 1977).

Sediment porosity was determined by drying known volumes of whole sediment at 80 °C to constant weight. The volume of pore water was calculated from the mass difference before and after drying after correcting for salt content.

3. RESULTS

3.1. Bulk POC

Bulk POC ranged from ~1.3 weight% (wt.%) to ~5.3 wt.% (Fig. 2a), and were about mid-range of bulk POC values reported previously for this site (Huh et al., 1987; Mollenhauer and Eglinton, 2007). POC was constant within the uppermost 2 cm of the sediment column at ~4.8 wt.%, but increased sharply by ~0.5 wt.% at 2.5 cm, then dropped to ~4.3 wt.% and remained largely unchanged to 20 cm (Fig. 2a; Table 2). A large discontinuity was present at 20 cm where POC dropped abruptly to ~1.4 wt.%. In agreement with past studies (Masiello and Druffel, 2003; Mollenhauer and Eglinton, 2007), $\Delta^{14}C_{POC}$ and $\delta^{13}C_{POC}$ also showed large changes across this horizon (Fig. 2b and c). Between ~5 and 18 cm, $\Delta^{14}C_{POC}$ decreased linearly (from about −150‰ to −200‰) consistent with radioactive decay (Fig. 2b), then dropped sharply across the discontinuity to about −460‰. Above 20 cm, $\delta^{13}C_{POC}$ ranged between −22.6‰ and −21.5‰, suggesting input of predominantly marine OC, but dropped to <−23.0‰ below 20 cm (Fig. 2c). In addition to these shifts, porosity (and by inference grain size), and total N:OC ratio also dropped across this horizon (Fig. 2d). Huh et al. (1987) report porosity profiles for this site that match closely with the present data. We interpret these changes to a switch in the sediment source due to the emplacement of a turbidite (Gorsline, 1996; Gorsline et al., 2000). The depth and timing of the discontinuity (20 cm corresponds to ~480 yrs since time of deposition using the sediment accumulation rate of Christensen et al. 1994), as well as the location of the sampling site, are consistent with an approximately 5 cm-thick turbidite-E reported by Gorsline et al. (2000).

The $\Delta^{14}C_{POC}$ profile showed a second discontinuity at ~2 cm, above which $\Delta^{14}C_{POC}$ was higher by ~40‰ due to incorporation of bomb-^{14}C into the sediments (Table 2; Williams et al., 1992; Pearson et al., 2000; Masiello and Druffel, 2003). Pre-bomb $\Delta^{14}C$ of surface-water DIC in this region is ~−80‰ (Williams et al., 1992; Ingram and Southon, 1996; Pearson et al., 2000).

3.2. POC compound classes

Roughly 50–70% of bulk POC was recovered as the sum of AI and TL fractions (Table 2, Fig. 2a). AI was the dominant fraction in all samples, and amounted to 44–61% of POC above the turbidite, and 70% of POC in the turbidite. A much smaller fraction of bulk POC was recovered as TL (~9% in the uppermost 3 cm, and 3–5% at depths >3 cm). These relative abundances of AI and TL agreed with those reported for other surface sediments of this region (Hwang et al., 2005; Komada et al., 2005).

$\Delta^{14}C_{AI}$ was lower than $\Delta^{14}C_{POC}$ by 13–46‰ (Table 2; Fig. 2b). Exclusive of the 0–0.5 cm depth interval where $\Delta^{14}C_{TL}$ and $\Delta^{14}C_{AI}$ overlapped, $\Delta^{14}C_{TL}$ was further depleted relative to $\Delta^{14}C_{AI}$ by 26‰ to as much as 270‰. Depletion in $\Delta^{14}C_{AI}$ and $\Delta^{14}C_{TL}$ relative to $\Delta^{14}C_{POC}$ was most pronounced within the turbidite. $\Delta^{14}C_{TL}$ also showed pronounced depletion within the 2–3 cm depth interval, al-

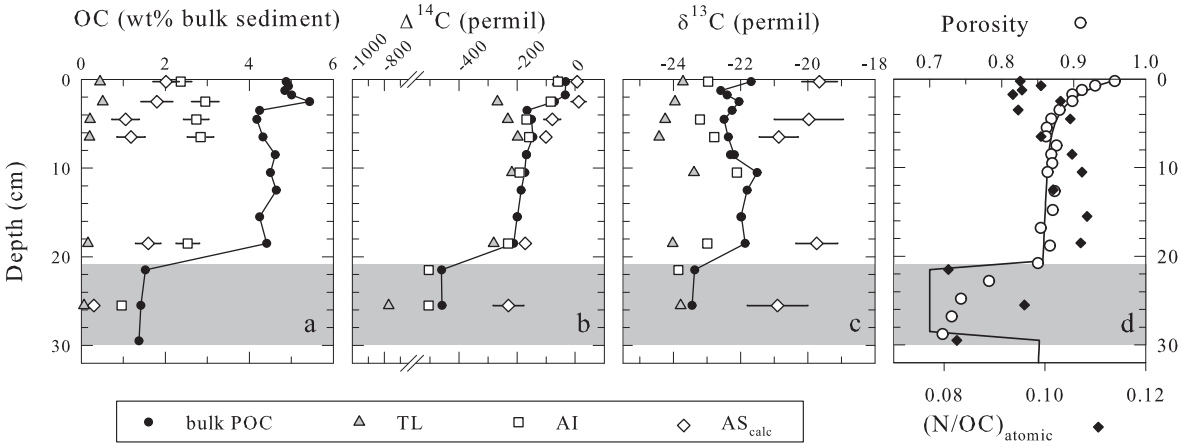

Fig. 2. (a) Concentration profiles of bulk POC, AI, TL, and AS_{calc} fractions in wt.% relative to bulk dry sediment mass, (b) $\Delta^{14}C$ signatures of bulk POC, AI, TL, and AS_{calc} fractions, (c) $\delta^{13}C$ signatures of bulk POC, AI, TL, and AS_{calc} fractions, and (d) porosity and atomic N/OC ratios in bulk sediment. Values for the AS_{calc} fraction were calculated from mass balance (Eqs. (1)–(3)), and shown with error bars that span the estimated lower and upper limits (see Section 3.2). Shaded areas indicate presence of a turbidite. The solid line in (d) is the modeled porosity (see Section 4.3.1).

beit to a smaller extent. The overall lower $\Delta^{14}C$ values of AI and TL fractions relative to POC indicated that the AS fraction had $\Delta^{14}C$ values higher than $\Delta^{14}C_{POC}$.

Similar to the trends in $\Delta^{14}C$, both $\delta^{13}C_{AI}$ and $\delta^{13}C_{TL}$ were consistently lower than $\delta^{13}C_{POC}$ (Table 2, Fig. 2c). $\delta^{13}C_{AI}$ was lower than $\delta^{13}C_{POC}$ by $\sim\leqslant 1‰$ throughout the profile. $\delta^{13}C_{TL}$ was lower than $\delta^{13}C_{POC}$ by ~2‰, except within the turbidite where the two values were within 0.5‰ of each other.

As stated in Section 2.2, all AS fractions were lost due to quartz tube failure during combustion. Therefore, the size and isotopic values of the AS fraction were estimated from POC, AI and TL data using the following equations:

$$(1-f)100 = \%AI + \%TL + \%AS_{calc} \quad (1)$$

$$(1-f)\Delta_{POC}100 = \Delta_{AI}\%AI + \Delta_{TL}\%TL + \Delta_{AS\text{-}calc}\%AS_{calc} \quad (2)$$

$$(1-f)\delta_{POC}100 = \delta_{AI}\%AI + \delta_{TL}\%TL + \delta_{AS\text{-}calc}\%AS_{calc} \quad (3)$$

Where %AI, %TL, and $\%AS_{calc}$ are the fraction (in %) of bulk POC recovered as AI, TL, and AS, respectively (Table 2), f is the fraction of the total POC that was lost during general sample processing ($0 \leqslant f < 1$; note that this is unrelated to the specific loss of the AS fraction), and Δ_i and δ_i are $\Delta^{14}C$ and $\delta^{13}C$ values of component i, respectively. The subscript 'calc' is used for all AS values to indicate that they were calculated by mass balance. Eqs. (1)–(3) assume that the $\Delta^{14}C$ and $\delta^{13}C$ values of any fractions that were lost during the extraction process were isotopically identical to those of bulk POC. Previous studies that applied the same extraction procedure to surface sediments from this region found that the bulk $\Delta^{14}C$ signature can be predicted to within ±80‰ by taking the weighted averages of the measured $\Delta^{14}C$ signatures of AI, TL and AS fractions (Hwang et al., 2005; Komada et al., 2005). With this assumption, values of $\%AS_{calc}$, $\Delta^{14}C_{AS\text{-}calc}$ and $\delta^{13}C_{AS\text{-}calc}$ were predicted in two ways: (1) by setting $f = 0$ to obtain the upper limit for $\%AS_{calc}$, and lower limits for $\Delta^{14}C_{AS\text{-}calc}$ and $\delta_{13}C_{AS\text{-}calc}$, and (2) by setting f equal to the maximum value (f_{max}) that yielded a positive $\%AS_{calc}$ value and $\Delta^{14}C_{AS\text{-}calc}$ and $\delta^{13}C_{AS\text{-}calc}$ signatures that were not prohibitively positive, to obtain the lower limit for $\%AS_{calc}$, and upper limits for $\Delta^{14}C_{AS\text{-}calc}$ and $\delta^{13}C_{AS\text{-}calc}$. This latter assumption resulted in $f_{max} = 0.2$ for the non-turbidite layers and $f_{max} = 0.1$ for the turbidite layer, both of which are within the range of loss estimates reported for surface sediments of this region (~0.3 or less; Hwang et al., 2005; Komada et al., 2005).

The calculated upper and lower limits of $\%AS_{calc}$ and isotopic values are shown in Table 2 and Fig. 2. $\%AS_{calc}$ ranged from 18% to 48%, with the highest average value observed in the 0–0.5 cm interval, and the lowest average value in the turbidite. $\Delta^{14}C_{AS\text{-}calc}$ ranged from −283‰ to +38‰, and were consistently higher than the corresponding bulk signatures. They were highest within the 0–3 cm interval where the bomb-^{14}C signal was evident, and decreased steadily with depth. $\delta^{13}C_{AS\text{-}calc}$ values were also consistently higher than corresponding bulk values, and ranged from −21.8‰ to −18.9‰. These observations are consistent with the AS fraction being enriched in modern marine OC relative to bulk POC.

3.3. Pore-water DOC and DIC

DOC increased across the sediment–water interface, formed a broad subsurface maximum in the top ~20 cm where it reached as high as 2 mM, then decreased with depth (Fig. 3). Comparison of DOC profiles from multiple cores collected from this site, including those from prior cruises to the same site (Burdige et al., 1999; Burdige, 2002), suggests that the size of this broad sub-surface maximum varies temporally and spatially, but that the DOC concentration at ~30 cm is near steady-state at around 0.8 mM. Also, no obvious gradient in DOC could be discerned below 30 cm. This was in contrast to DIC, which increased steadily with depth, and was highly linear below

Table 2
Carbon content and isotopic values of bulk POC and organic compound classes. All samples were collected from core 9–7. Estimated uncertainties are: wt.% POC $\leqslant \pm 0.05$ wt.%; $\Delta^{14}C_{POC} \pm 1$–2‰; $\Delta^{14}C_{AI} \pm 1$–3‰; $\Delta^{14}C_{TL} \pm 1$–3‰; $\delta^{13}C_{POC} \pm 0.1$‰; $\delta^{13}C_{AI} \pm 0.2$‰; $\delta^{13}C_{TL} \pm 0.2$‰.

Depth interval (cm)	POC				AI				TL				AS_{calc}[c]		
	SFSU[a]	(wt.%)	$\Delta^{14}C$ (‰)	$\delta^{13}C$ (‰)	SFSU	%AI[b]	$\Delta^{14}C$ (‰)	$\delta^{13}C$ (‰)	SFSU	%TL[b]	$\Delta^{14}C$ (‰)	$\delta^{13}C$ (‰)	%AS_{calc}	$\Delta^{14}C$ (‰)	$\delta^{13}C$ (‰)
0.0–0.5	513	4.83	−33	−21.7	622	44	−59	−23.0	575	8	−61	−23.7	35–48	−4 to +17	−20.2 to −19.1
1.0–1.5	515	4.68		−22.6											
1.5–2.0	516	4.87	−34	−22.4											
2.0–3.0	517	5.26	−71	−22.0	623	50	−84		571	9	−268	−24.0	27–42	−14 to +38	
3.0–4.0	512	4.11	−166	−22.3											
4.0–5.0	458	3.99	−150	−22.5	624	61	−168	−23.2	576	5	−232	−24.2	18–35	−108 to −50	−21.0 to −18.9
6.0–7.0	459	4.22	−146	−22.4	625	60	−159	−22.8	572B	4	−198	−24.4	20–36	−118 to −84	−21.4 to −20.3
8.0–9.0	460	4.51	−168	−22.2											
	467	4.53	−168	−22.3											
10.0–11.0	461	4.36	−174	−21.5	626		−192	−22.1	577	5	−218	−23.4			
12.0–13.0	462	4.56	−186	−21.8											
15.0–16.0	463	4.04	−199	−22.0											
	499	4.11	−200	−22.0											
18.0–19.0	468	4.29	−212	−21.9	627	53	−231	−23.0	573A	3	−280	−24.0	30–44	−184 to −161	−20.4 to −19.1
21.0–22.0	508	1.44	−460	−23.4	628	70	−504	−23.9							
25.0–26.0	509	1.33	−459	−23.4	629	69	−505		574	5	−773	−23.8	18–27	−283 to −177	−21.8 to −20.0[d]

[a] Internal identification number.
[b] Fraction (in %) of bulk POC recovered as AI or TL.
[c] All AS values were calculated by mass balance using Eqs. (1)–(3) as described in the text. Estimated ranges were calculated by assuming that up to 20% of POC was lost during processing, except for the 25–26 cm horizon for which a 10% loss was assumed (an assumption of a 20% loss rate resulted in unacceptable values).
[d] Calculated by assuming that the $\delta^{13}C$ of SFSU629 was identical to that of SFSU628.

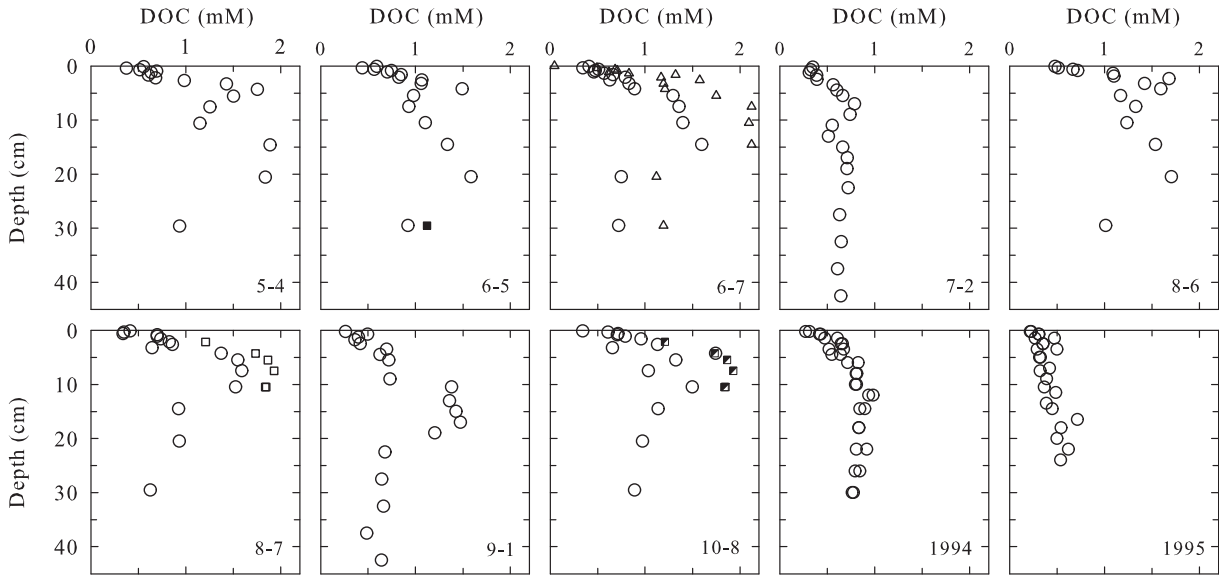

Fig. 3. Pore water DOC profiles obtained by HTC (open circles), UV_{ox} (triangles), and TSR (filled, open, and diagonally-filled squares). Numbers in each panel are core IDs (cast number–core number). DOC profiles from the same site collected in 1994 and 1995 are also shown (Burdige et al., 1999; Burdige, 2002).

~10 cm, indicating upward diffusion of DIC from deeper horizons (Burdige and Komada 2011).

DOC concentrations determined by HTC were consistently lower than DOC determined by UV_{ox} and TSR (Fig. 3). Because this comparison was made only using splits from frozen samples, it is possible that this offset arose from precipitate formation, and the fact that these precipitates tend to be under-sampled during analysis by HTC (Alperin and Martens, 1993; Johnson and Komada, 2011). DOC concentrations in refrigerated samples which did not form precipitates were also relatively low (cores 7–2 and 9–1; Fig. 3). The cause for this is unclear, but could be due to spatial heterogeneity, because DOC loss during refrigerated storage of acidified samples in ampoules has been observed to be minimal, at least for oligotrophic surface ocean waters (Tupas et al., 1994). Because of this variability in DOC profiles, in the model discussed below, we use only UV_{ox}- and TSR-derived DOC concentration data from cores 6–5, 6–7, 8–7, and 10–8 for which isotopic values are also available (Fig. 4a).

$\Delta^{14}C_{DOC}$ increased sharply across the sediment–water interface, from a bottom-water value of −504‰ to as high as −35‰ in the upper 2 cm, then dropped to ~−240‰ by 30 cm (Fig. 4b and h; Table 3). These values were higher than $\Delta^{14}C_{DOC}$ previously reported for this site (−462‰ to −186‰ between 0.125 and 5.5 cm; Bauer et al., 1995). $\delta^{13}C_{DOC}$ values were ~−22‰ near the surface and ~−23.5‰ at 30 cm (Fig. 4c and i). There was considerable inter- and intra-core variability in $\delta^{13}C_{DOC}$ in the uppermost 10 cm of the sediment column, but values converged at depth. $\Delta^{14}C_{DIC}$ exhibited a similar depth trend as $\Delta^{14}C_{DOC}$, but the magnitude of the change was significantly attenuated (total variability of ~50‰ compared to ~200‰ for $\Delta^{14}C_{DOC}$; Fig. 4e and k). $\delta^{13}C_{DIC}$ decreased in an exponential fashion from −0.9‰ in the bottom water to −15.5‰ at 30 cm depth (Fig. 4f and l). $\delta^{13}C_{DOC}$, $\delta^{13}C_{DIC}$, and $\Delta^{14}C_{DIC}$ values overlapped with those reported previously for this site (Bauer et al., 1995; Berelson and Stott, 2003).

4. DISCUSSION

4.1. POC composition inferred from organic fractions data

Sediments of the inner California Borderland Basins receive POC from various sources with variable C-isotopic signatures. Land-derived POC includes modern biomass and fossil carbon from bedrock weathering and anthropogenic petroleum contamination (Pearson and Eglinton, 2000; Hwang et al., 2005; Komada et al., 2005). ^{14}C and ^{13}C analyses of specific biomarkers further show that OC produced by terrestrial and marine ecosystems in this region can undergo substantial aging in intermediate reservoirs (such as soils and the continental shelf) prior to reaching the site of permanent burial (Mollenhauer and Eglinton, 2007; Shah et al., 2008; Drenzek et al., 2009). Although $\delta^{13}C$ values of bulk POC in surface SMB sediments show little variability (~−22‰ to −24‰; Fig. 2; Williams et al., 1992; Gong and Hollander, 1997), $\delta^{13}C$ values of specific lipid biomarkers show much greater variability (~−18‰ to <−40‰) reflecting the heterogeneity in end-member OC sources (Gong and Hollander, 1997; Pearson et al., 2001; Mollenhauer and Eglinton, 2007).

The relative abundances and isotopic values of organic compound classes extracted from SMB sediments were consistent with the presence of variable end-member POC sources to this site. Within the 0–3 cm depth interval, both %TL and $\%AS_{calc}$ were elevated relative to deeper horizons (Table 2). The high $\%AS_{calc}$ in this depth interval likely reflects the presence of relatively fresh marine-derived OC, as inferred from the high values of $\Delta^{14}C_{AS\text{-}calc}$ and $\delta^{13}C_{AS\text{-}calc}$ (Fig. 2b and c). In contrast, high %TL in this depth region appears to be affected by input of fossil lipids

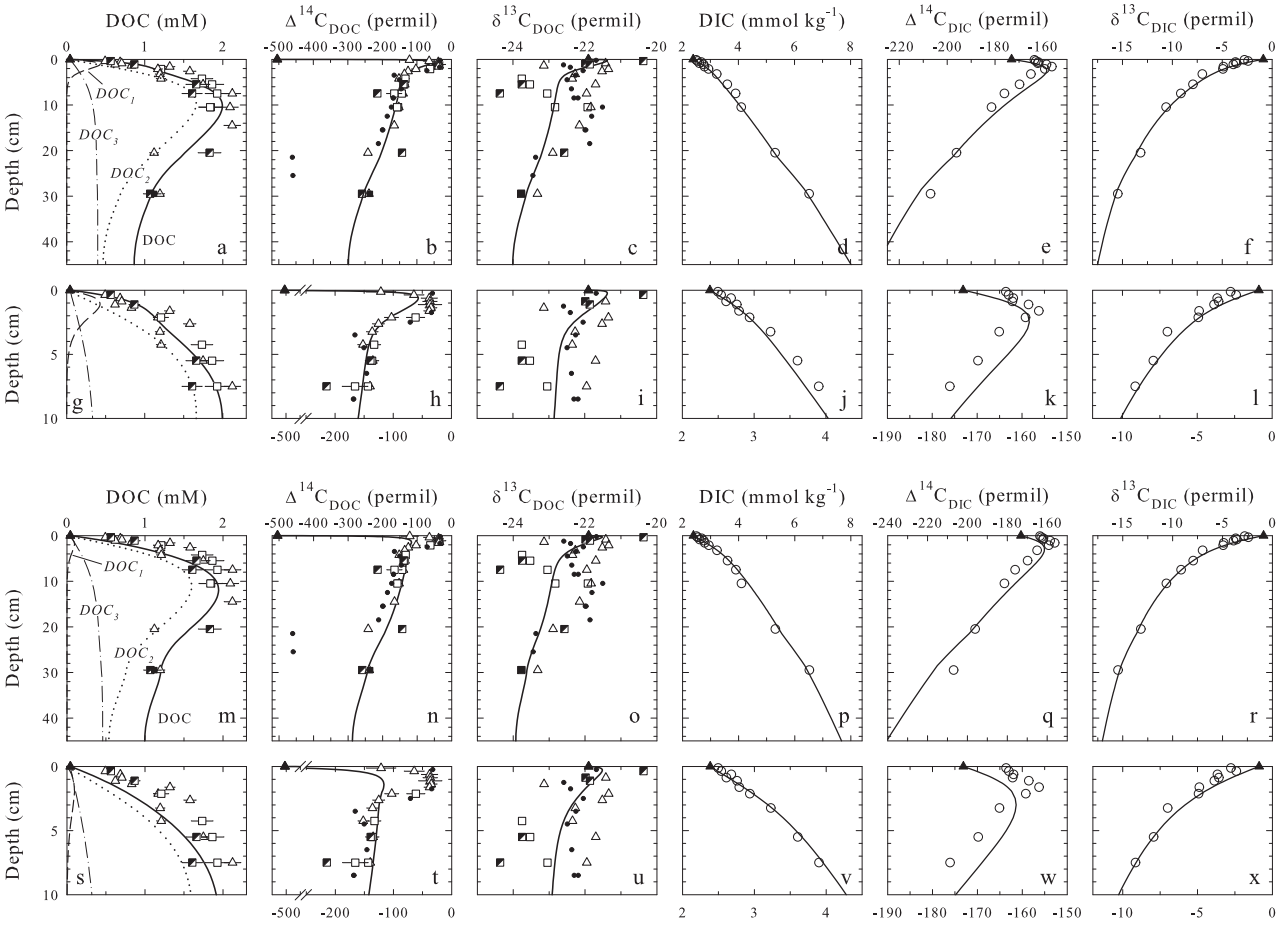

Fig. 4. Pore water profiles of measured values (symbols) and model results (lines). Panels (a–l) show results from model *run-A*, and panels (m–x) show results from model *run-B*. The left three columns show DOC and its isotopic compositions from cores 6–5 (solid squares), 6–7 (open triangles), 8–7 (open squares), and 10–8 (diagonally-filled squares). The right three columns show DIC and its isotopic compositions from core 11–6. The 2nd and 4th rows are expanded views of the top 10 cm of the 1st and 3rd rows, respectively. In the first column, model results for DOC sub-fractions (DOC_1, DOC_2, and DOC_3) are shown along with modeled bulk DOC. In second and third columns, POC data from Fig. 2 are shown in small black circles for comparison. Filled triangles are bottom water values. Where error bars are not visible, they are smaller than the symbols.

in addition to surface production, because the subsurface maximum in %TL between 2 and 3 cm coincided with a local minimum in $\Delta^{14}C_{TL}$. This is consistent with the work of Pearson and Eglinton (2000) which shows higher levels of petroleum-derived *n*-alkanes in the 0–2.5 cm horizon relative to the 2.5–7.5 cm depth interval at this site.

Between 3 and 20 cm, %AI, %TL and $\%AS_{calc}$ did not change significantly with depth (Table 2). Isotopic values of these fractions also tended to parallel those of POC with little variability (Fig. 2b and c). However, across the 20 cm discontinuity, $\Delta^{14}C_{AI}$ and $\Delta^{14}C_{TL}$ dropped abruptly, with this shift being particularly pronounced for $\Delta^{14}C_{TL}$ (almost 500‰). $\delta^{13}C_{POC}$ also dropped from −21.9‰ to −23.4‰, while %AI increased from 53% to 70%. These shifts are consistent with the turbidite layer being enriched in highly reworked, pre-aged material relative to the overlying 0–20 cm section of hemipelagic material. In contrast, $\Delta^{14}C_{AS\text{-}calc}$ decreased steadily across the 20 cm discontinuity at a rate similar to that observed between 3 and 20 cm. These results suggest that the composition of AI and TL fractions differ significantly between sediments that are supplied to the site via vertical particle flux versus those delivered through major lateral transport events. On the other hand, the composition of the AS fraction appears relatively insensitive to changes in the mode of sediment transport, consistent with this fraction originating mostly from recent surface marine production.

The values of $\delta^{13}C_{TL}$ and $\delta^{13}C_{AS\text{-}calc}$ differed by ~4‰ throughout the core (Fig. 2c). This offset is consistent with isotopic fractionation associated with biosynthesis of these compound classes (Degens et al., 1968; DeNiro and Epstein, 1977). In contrast, the much larger differences between $\Delta^{14}C_{TL}$ and $\Delta^{14}C_{AS\text{-}calc}$ (from ~50‰ to as much as ~550‰ in the turbidite) indicate variable amounts of fossil- and/or pre-aged OC in the TL fraction.

4.2. Qualitative analysis of pore-water DOC isotopic composition

Throughout the core, $\delta^{13}C_{DOC}$ values generally fell within ±1‰ of $\delta^{13}C_{POC}$ and $\delta^{13}C_{AI}$ (Fig. 4c and i; Tables 2 and 3), suggesting that DOC was similar to bulk POC and the

Table 3
Summary of the concentrations and $\Delta^{14}C$ and $\delta^{13}C$ signatures of pore-water DIC and DOC for cores 11–6, 6–7, 8–7, and 10–8 (cast number–core number). Estimated uncertainties are: DIC $\leqslant \pm 2\%$; $DOC_{UV_{ox}} \pm 5\%$; $DOC_{TSR} \pm 8\%$; $\Delta^{14}C_{DIC} \pm 3‰$; $\delta^{13}C_{DIC} \pm 0.1‰$; $\delta^{13}C_{UVox} \pm 0.4‰$; $\delta^{13}C_{TSR} \pm 0.4‰$. Uncertainties for $\Delta^{14}C$ of DOC processed by UV_{ox} ($DOC_{UV_{ox}}$) are from the UCI Keck CCAMS report; those for DOC processed by TSR (DOC_{TSR}) were derived following Hwang and Druffel (2005).

Depth interval (cm)	DIC Core 11–6				$DOC_{UV_{ox}}$ Core 6–7						DOC_{TSR} Core 8–7						DOC_{TSR} Core 10–8					
	SFSU[a]	DIC (mmol kg^{-1})	$\Delta^{14}C$ (‰)	$\delta^{13}C$ (‰)	UCID[a]	DOC (mM)	C[b] (μg)	$\Delta^{14}C$ (‰)	± (‰)	$\delta^{13}C$ (‰)	SFSU[a]	DOC (mM)	C[b] (μg)	$\Delta^{14}C$ (‰)	± (‰)	$\delta^{13}C$ (‰)	SFSU[a]	DOC	C[b] (μg)	$\Delta^{14}C$ (‰)	± (‰)	$\delta^{13}C$ (‰)
BW[c]	601A	2.386	−173	−0.89	12643	0.045	375	−504	3	−21.9												
0.00–0.25	354	2.50	−164	−2.78	12728		50	−121	25	−23.7												
0.25–0.50	391	2.54	−163	−2.41	12729	0.493	75	−64	17	−22.4							773	0.56	–[d]	–[d]		−20.4
0.50–0.75	386	2.68	−162	−3.67	12730	0.685	98	−38	14	−22.5												
0.75–1.00	390	2.61	−162	−3.57	12810	0.705	108	−37	12	−21.4							774		–[d]	–[d]		−22.0
1.00–1.25	387	2.76	−159	−3.88	12727	0.619	67	−37	20	−23.8							775	0.87	–[d]	–[d]		−21.9
1.25–1.50					12724	0.830	138	−35	10	−23.1												
1.50–1.75	357	2.79	−156	−4.88	12723	1.321	144	−38	9													
2.00–2.25	366	2.94	−159	−4.94	12450	1.168	216	−114	12	−21.3	740	1.21	239	−60	16							
2.50–2.75				−6.10	12722	1.578	121	−125	10	−21.5												
3.00–3.50	382	3.23	−165	−7.00	12451	1.196	251	−142	10	−22.3												
4.0–4.5				−7.14	12416	1.209	272	−157	9	−22.3	769	1.73	332	−133	11	−23.8						
5.0–6.0	352	3.60	−170	−7.94	12454	1.748	611	−138	7	−21.7	770	1.86	321	−136	12	−23.5	748	1.66	414	−139	9	−23.8
7.0–8.0	383	3.90	−176	−9.15	12418	2.123	752	−140	3	−22.0	771	1.93	411	−144	8	−23.0	747	1.61	520	−217	7	−24.4
											792	1.18	171	−167	22	–						
10.0–11.0	374	4.16	−181	−10.63	12421	2.094	755	−152	4	−21.8	791	1.84	247	−158	15	−22.8						
	414	4.10	−182																			
14.5–15.0				−11.83	12458	2.121	812	−166	4	−22.2												
20.0–21.0	345	5.31	−196	−13.19	12456	1.121	320	−242	5	−22.9							746	1.83	687	−144	5	−22.6
29.0–30.0	384	6.52	−207	−15.48	12811	1.195	262	−239	5	−23.3							594[e]	1.12	217	−227	6	−23.8
																	620	1.07	309	−253	4	−23.8

[a] Internal identification numbers.
[b] Amount of carbon in the $\Delta^{14}C$ split.
[c] Bottom water collected from Go Flo bottle.
[d] Sample size was insufficient for $\Delta^{14}C$ analysis.
[e] SFSU#594 was taken from core 6–5 at the specified depth interval.

AI fraction in chemical composition. $\Delta^{14}C_{DOC}$ values were also similar to $\Delta^{14}C_{POC}$ and $\Delta^{14}C_{AI}$ between 0 and 10 cm (Fig. 4h; Tables 2 and 3). However, below 10 cm, $\Delta^{14}C_{DOC}$ generally exceeded $\Delta^{14}C_{POC}$ (Fig. 4b), suggesting preferential dissolution of younger components of bulk POC to DOC with increasing depth. It should be noted that while $\Delta^{14}C_{DOC}$ values were similar to $\Delta^{14}C_{AS\text{-}calc}$ at depths > 10 cm, $\delta^{13}C_{AS\text{-}calc}$ exceeded $\delta^{13}C_{DOC}$ by ~2‰ throughout the core (Tables 2 and 3), suggesting that the AS fraction was not a major source of the pore-water DOC standing stock. We later show through modeling that the AS fraction was likely involved in POC remineralization via DOC intermediates, but that this DOC did not accumulate to any significant extent in the pore water because of its efficient oxidation to DIC.

The ~200‰ drop in $\Delta^{14}C_{DOC}$ in the uppermost 30 cm of the sediment column (Fig. 4b) provides additional clues with regards to pore-water DOC composition. Assuming a whole sediment diffusion coefficient for DOC of 44.6 $cm^2\ yr^{-1}$ (Burdige et al., 1992, 1999; Alperin et al., 1994) the time scale for DOC to diffuse over the distance covered by these cores is on the order of a decade, which is far too short for radioactive decay to cause any detectable decrease in $\Delta^{14}C$ ($t_{1/2} = 5730$ yr). Therefore, this drop in $\Delta^{14}C_{DOC}$ is better explained by depth-dependent differential turnover of sub-pools of DOC with distinct $\Delta^{14}C$ values. The maximum in $\Delta^{14}C_{DOC}$ in the uppermost 2 cm is consistent with production of DOC from POC containing bomb-^{14}C, and the presence of a corresponding peak in $\Delta^{14}C_{DIC}$ shows that this DOC was rapidly oxidized to DIC; i.e., that it was labile (Fig. 4e and k). The large decrease in $\Delta^{14}C_{DOC}$ below this peak indicates that ^{14}C-rich DOC was largely confined to the surface sediments, and that bulk DOC became increasingly dominated by relatively ^{14}C-depleted material with depth. These observations are consistent with net accumulation of $\Delta^{14}C$-depleted DOC reported previously for a sediment incubation experiment (Komada et al., 2012), and strongly suggest that bulk DOC consists of at least two sub-pools with distinct isotopic compositions and reactivities.

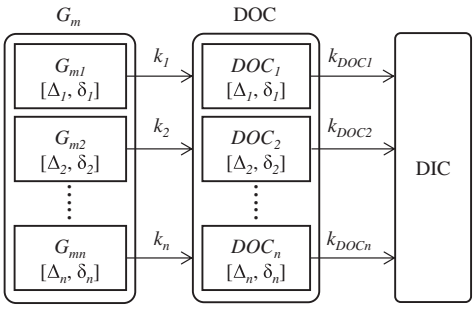

Fig. 5. Selective degradation model used to simulate pore-water DOC profiles. Metabolizable fraction of bulk POC (G_m) is divided into n components, each with its unique degradation rate constant (k_i) and $\Delta^{14}C$ and $\delta^{13}C$ signatures (Δ_i and δ_i, respectively, where $1 \leqslant i \leqslant n$). G_{mi} is solubilized to DOC_i without isotopic fractionation; DOC_i is then oxidized to DIC without isotopic fractionation. Degradation rates are assumed to be first order with respect to G_{mi} and DOC_i. In this study, n was set equal to 3.

4.3. Analysis of pore-water DOC using a selective degradation model

4.3.1. Model description

A selective degradation model is proposed to further interpret the data, and to explore the presence of isotopically and kinetically distinct pools of pore-water DOC (Fig. 5). Conceptually, this model is an extension of the multi-G model of Westrich and Berner (1984) that here includes DOC, and tests the idea that isotopically and kinetically heterogeneous DOC is produced and consumed during remineralization of multiple pools of metabolizable organic matter (G_m). There are $\geqslant 2$ pools of G_{mi}, each characterized with distinct $\Delta^{14}C$ and $\delta^{13}C$ signatures (Δ_i and δ_i). It is assumed that DOC_i is produced by first-order degradation of G_{mi} with degradation rate constant k_i, and that DOC_i has the same isotopic values as its parent. This DOC_i is then oxidized without isotopic fractionation to DIC (Boehme et al., 1996; Penning and Conrad, 2006) with rate constant k_{DOC_i}. These kinetics were implemented in a steady-state, variable-porosity, reactive transport model for carbon species only for the uppermost 45 cm of the sediment column (Tables 4 and 5, Eqs. (4)–(10)). DOC concentrations showed

Table 4
Equations used in the selective utilization model.

DOC

$$DOC = \sum_{i=1}^{3} DOC_i \quad (4)$$

$$\frac{1}{\varphi}\frac{\partial}{\partial x}\left(\varphi D_s^{DOC}\frac{\partial DOC_i}{\partial x}\right) + Fk_i G_{mi} - k_{Di} DOC_i = 0 \quad (5)$$

$$\frac{1}{\varphi}\frac{\partial}{\partial x}\left(\varphi D_s^{DOC}\frac{\partial DO^{13}C_i}{\partial x}\right) + Fk_i G_{mi}^{13} - k_{Di} DO^{13}C_i = 0 \quad (6)$$

$$\frac{1}{\varphi}\frac{\partial}{\partial x}\left(\varphi D_s^{DOC}\frac{\partial DO^{14}C_i}{\partial x}\right) + Fk_i G_{mi}^{14} - (k_{Di} + \lambda) DO^{14}C_i = 0 \quad (7)$$

DIC

$$\frac{1}{\varphi}\frac{\partial}{\partial x}\left(\varphi D_s^{DIC}\frac{\partial DIC}{\partial x}\right) + \sum_{i=1}^{3} k_{Di} DOC_i = 0 \quad (8)$$

$$\frac{1}{\varphi}\frac{\partial}{\partial x}\left(\varphi D_s^{DIC}\frac{\partial DI^{13}C}{\partial x}\right) + \sum_{i=1}^{3} k_{Di} DO^{13}C_i = 0 \quad (9)$$

$$\frac{1}{\varphi}\frac{\partial}{\partial x}\left(\varphi D_s^{DIC}\frac{\partial DI^{14}C}{\partial x}\right) - \lambda DI^{14}C + \sum_{i=1}^{3} k_{Di} DO^{14}C_i = 0 \quad (10)$$

D_s^j is the whole sediment diffusion coefficient for species j (see Appendix A), while λ is the decay constant for ^{14}C based on the new half-life (Stuiver and Polach, 1977). F is a factor that converts concentration in units of wt.% to mM, and is defined as $F = (\rho_{sed}/12) \times ((1-\varphi)/\varphi) \times 10^4$, where ρ_{sed} is the dry sediment density (assumed to be 2.65), and φ is the porosity (see Eq. (13)). Since φ is a function of depth, so is F. G_{mi}^{13} and G_{mi}^{14} are metabolizable $PO^{13}C$ and $PO^{14}C$, respectively, and are defined in Appendix A.

Table 5
Model parameters with prescribed values.

Parameter	Description	Value	Units	Source
DIC_0	Bottom-water DIC concentration	2.39	mM	This study
DOC_0	Bottom-water DOC concentration	45	μM	This study
$\delta^{13}{}_{DIC_0}$	$\delta^{13}C$ value of bottom-water DIC	−0.89	‰	This study
$\Delta^{14}{}_{DIC_0}$	$\Delta^{14}C$ value of bottom-water DIC	−173	‰	This study
$\delta^{13}C_{DOC_0}$	$\delta^{13}C$ value of bottom-water DOC	−21.9	‰	This study
$\Delta^{14}C_{DOC_0}$	$\Delta^{14}C$ value of bottom-water DOC	−504	‰	This study
D_0^{DIC}	DIC seawater free solution diffusion coefficient	194.1	$cm^2\ yr^{-1}$	See footnote a
D_0^{DOC}	DOC seawater free solution diffusion coefficient	51	$cm^2\ yr^{-1}$	See footnote b
W	Mass flux to the sediments	0.013	$g\ cm^{-2}\ yr^{-1}$	Christensen et al. (1994)

[a] Determined as a weighted average of the $D°$ values for HCO_3^-, CO_3^{2-}, and aqueous CO_2 based on their relative average composition ($\pm 1\sigma$) in pore water DIC from Santa Monica Basin sediments ($93.7 \pm 2.8\%$, $3.8 \pm 3.5\%$, and $3.5 \pm 2.1\%$, respectively; $D°$ values for bicarbonate, carbonate and aqueous CO_2 were obtained from Schulz and Zabel (2006) for an assumed bottom water temperature of 5 °C).

[b] Determined using an empirical relationship between $\log D°$ and log molecular weight for known dissolved organic compounds (Burdige et al., 1992; Alperin et al., 1994) assuming that the molecular weight of DOC in porewaters ranged from 0.5 to 5 kDa with a log-average weight of 1.6 kDa.

temporal and spatial variations (Fig. 3), but the general agreement in both concentration and isotopic values among three cores collected in 2008 (Fig. 4a–f) justifies the assumption of steady-state for these calculations. The assumption of steady-state is discussed further below.

A multi-G model was used here over a 1-G model, because it is difficult to explain the asymptotic, non-zero DOC concentration at depth when only one pool of G_m is present (Burdige, 2006). Specifically, establishment of non-zero asymptotic DOC concentrations at depth requires that either: (i) DOC becomes increasingly recalcitrant with depth, or (ii) DOC production equals DOC consumption at depth (Komada et al., 2004; Burdige, 2006). As discussed elsewhere (Burdige and Komada, 2011), it is unlikely that these sediments meet condition (ii). Furthermore, geopolymerization-type reactions that transform reactive DOC components produced from a single G_m precursor into more refractory components are likely to be too slow as compared to the time scales of pore water diffusion or remineralization of these reactive DOC components (e.g., Alperin et al., 1994). We therefore explored condition (i) using a multi-G model (DOC production pathway-(b) in Fig. 1).

In developing this model we recognize that sedimentation in SMB has varied in time due to episodic deposition of turbidites (Gorsline et al., 2000). Deposition of POC has an additional time-dependent component given that surface-water derived POC deposited to the sediments after ~1960 contains bomb-^{14}C (McNichol and Aluwihare, 2007). Despite this temporal variability with respect to deposition of solid material, we also note that pore water profiles in general approach quasi-steady state relatively rapidly with respect to such time-dependent profiles (see Burdige (2006) and discussions therein). We therefore used a modified steady-state approach to define the instantaneous depth profiles for each of the G_m pool components (i.e., total carbon, ^{13}C and ^{14}C of each G_m pool), then used these depth profiles to define the depth distribution of DOC_i production in the sediments. These were then incorporated into steady-state solutions to the DOC and DIC equations given in Table 4. This approach is described in detail in Appendix A.

The data were best explained with three pools of G_m (G_{m1}, G_{m2}, and G_{m3}), each generating DOC_1, DOC_2, and DOC_3. Bulk DOC was modeled as the sum of these DOC_i pools (Eq. (4)). DIC was calculated by summing the DIC generated from the oxidation of DOC_i (Eq. (4)). $\delta^{13}C$ and $\Delta^{14}C$ profiles of DOC and DIC were derived by solving analogous equations for ^{13}C and ^{14}C, although equations for $DO^{14}C_i$ and $DI^{14}C$ included radioactive decay as additional loss terms (Eqs. (6), (7), (9) and (10)). Model-derived ^{13}C and ^{14}C concentrations for DOC and DIC at a given depth, x, were converted to $\delta^{13}C$ and $\Delta^{14}C$ values of DOC and DIC as:

$$\delta^{13}C(x) = 1000\left(\frac{\left(\frac{^{13}C}{^{12}C}\right)_x}{R_{PDB}} - 1\right) \tag{11}$$

$$\Delta^{14}C(x) = 1000\left[\left(\frac{\left(\frac{^{14}C}{^{12}C}\right)_x}{R_{abs}} \cdot \left\{\frac{1 + 0.001 \cdot (-25)}{1 + 0.001 \cdot \delta^{13}C(x)}\right\}^2\right) \cdot \exp\left(\frac{1950 - y}{8267}\right) - 1\right]$$

$$= 1000\left[F_m \cdot \exp\left(\frac{1950 - y}{8267}\right) - 1\right] \tag{12}$$

where $(^{13}C/^{12}C)_x$ and $(^{14}C/^{12}C)_x$ are the isotopic ratios of DOC or DIC at depth x, R_{PDB} is the $^{13}C/^{12}C$ ratio of the PDB standard, R_{abs} is the ^{14}C/(total C) ratio of the absolute radiocarbon standard, and y is the year of sample collection. The F_m term in Eq. (12) is the fraction modern value, which is the $\delta^{13}C$-normalized fractional abundance of ^{14}C in the sample relative to that in the absolute radiocarbon standard (Stuiver and Polach, 1977; McNichol and Aluwihare, 2007).

Known bottom-water values were used to define the boundary conditions of the model equations at $x = 0$ cm (Table 5). A constant-flux condition was applied at the base of the model (45 cm) for DIC, $DI^{14}C$ and $DI^{13}C$, although the values of the fluxes were used as adjustable fitting parameters. Concentration gradients of DOC, $DO^{14}C$ and

$DO^{13}C$ were assumed to approach zero at 45 cm. It is clear from the dataset that $\Delta^{14}C_{DOC}$ and $\delta^{13}C_{DOC}$ profiles that penetrate deeper into the sediments are needed to assess the validity of this assumption.

Depth-dependent porosity (Fig. 2) was used in these model equations in part to account for the impact of a steep porosity gradient near the sediment surface (due to sediment compaction) on solid phase POC profiles, and in part to incorporate any effects of the presence of the low porosity turbidite on diffusive transport through the sediment column. In spite of these concerns, model results using fixed versus variable porosity were not significantly different. For completeness, we show the variable porosity results here.

The following porosity distribution was used in our model,

$$\varphi = \begin{cases} p_1 + p_2 e^{-p_3 x} - p_4 x & (x < zt_{top}) \\ \varphi_{tur}\ (zt_{bot} \geqslant x \geqslant zt_{top}) \\ p_1 + p_2 e^{-p_3 x} - p_4 x & (x > zt_{bot}) \end{cases} \quad (13)$$

where $zt_{top} = 21$ cm, $zt_{bot} = 29$ cm, $\varphi_{tur} = 0.7$, and p_1 to p_4 are fitting parameters that were obtained by fitting the first row of Eq. (13) to the porosity data at depths $< zt_{top}$ ($p_1 = 0.87$, $p_2 = 0.09$, $p_3 = 0.48\ cm^{-1}$, and $p_4 = 0.00055\ cm^{-1}$; Fig. 2d). For model data points above zt_{top} or below zt_{bot} the first derivative of φ (see Appendix A for details) was determined using,

$$\frac{d\varphi}{dx} = -p_2 p_3 e^{-p_3 x} - p_4 \quad (14)$$

while for model data points in the turbidite section, we assumed this derivative was equal to zero. Across the upper and lower turbidite boundaries, $\frac{d\varphi}{dx}$ was obtained numerically using a centered, finite-difference approximation applied to the set of φ (versus x) values calculated with Eq. (13).

The model equations for DOC and DIC in Table 4 were solved numerically after expanding the diffusive terms in these equations as described in Appendix A. Centered-finite differencing schemes were used to approximate the first and second derivatives in these equations (Boudreau 1997), and to better capture the finer details of the profiles near the sediment–water interface, an uneven grid was used whereby Δx increased from 0.005 to 1 cm as a function of depth. For each solute, this approach resulted in an equation at each grid point from 0 to 45 cm. Each set of these equations for a given solute was expressed in matrix form and solved in MATLAB by Gaussian elimination. Isotopic concentrations were converted back to $\Delta^{14}C$ and $\delta^{13}C$ values using Eqs. (11) and (12) prior to the fitting process described below.

For a given starting set of the 19 fitting parameters (Table 6) six r^2 values were obtained by fitting the model equations to the concentrations and isotopic signatures of DOC and DIC. The best fit of the model to the complete data set was obtained by varying these fitting parameters to minimize the average of the six $1 - r^2$ values (referred to here as *err*). This was carried out in MATLAB using the routine *fminsearch*.

Table 6
Adjustable model parameters and their best-fit values.

Parameter	Description	*run-A*[a]		*run-B*[a]		Units
		Best fit value	Error	Best fit value	Error	
G_{m1}	Metabolizable POC; highest lability	6.5	0.9	3.2	0.6	wt.%
G_{m2}	Metabolizable POC; intermediate lability	1.9	0.2	2.0	0.4	wt.%
G_{m3}	Metabolizable POC; lowest lability	0.18	0.08	0.14	0.08	wt.%
k_1	Degradation rate constant for G_{m1}	0.10	0.02	2.1×10^{-2}	0.3×10^{-2}	yr^{-1}
k_2	Degradation rate constant for G_{m2}	0.7×10^{-2}	0.1×10^{-2}	4.2×10^{-3}	0.9×10^{-3}	yr^{-1}
k_3	Degradation rate constant for G_{m3}	$(=k_2)$[b]		$(=k_2)$[b]		yr^{-1}
k_{DOC_1}	Degradation rate constant for DOC_1	33	9	80	36	yr^{-1}
k_{DOC_2}	Degradation rate constant for DOC_2	0.16	0.06	0.23	0.09	yr^{-1}
k_{DOC_3}	Degradation rate constant for DOC_3	0.9×10^{-4}	0.5×10^{-4}	1.0×10^{-4}	0.6×10^{-4}	yr^{-1}
Δ_1	$\Delta^{14}C$ value of G_{m1}	+48	25	+68	43	‰
Δ_{1pre}	$\Delta^{14}C$ value of G_{m1}, pre-bomb	−52	40	−58	33	‰
Δ_2	$\Delta^{14}C$ value of G_{m2}	−66	26	−45	23	‰
Δ_3	$\Delta^{14}C$ value of G_{m3}	−520	180	−480	190	‰
δ_1	$\delta^{13}C$ value of G_{m1}	−20.6	0.2	−17	1	‰
δ_2	$\delta^{13}C$ value of G_{m2}	−22.2	0.1	−22.4	0.1	‰
δ_3	$\delta^{13}C$ value of G_{m3}	−27	2	−26	3	‰
$\Delta_{lb\text{-}DIC}$	$\Delta^{14}C$ value of DIC flux at lower boundary	−310	20	−390	70	‰
$\delta_{lb\text{-}DIC}$	$\delta^{13}C$ value of DIC flux at lower boundary	−25.4	0.6	−26	3	‰
$J_{lb,DIC}$	Diffusive flux of DIC at lower boundary	−0.32	0.03	−0.24	0.06	$mmol\ m^{-2}\ d^{-1}$
$J_{lb,DOC}$	Diffusive flux of DOC at lower boundary	(0.00)[c]		(0.00)[c]		$mmol\ m^{-2}\ d^{-1}$

[a] *run-A* is the default model run. *run-B* includes the empirical relationship between benthic DOC and DIC fluxes (Eq. (15)) as an additional fitting constraint.

[b] To minimize the number of unknown fitting parameters, k_2 and k_3 were set equal to one another. Preliminary model runs in which they were not set equal to each other resulted in values that were within error of each rate constant. No significant differences were seen in the other fitting parameters using either approach.

[c] Prescribed (no-flux lower boundary condition).

Given the large number of fitting parameters in the model it was important to ensure that the fitting process found a "global" (versus "local") minimum value of *err*. This was carried out using a Monte Carlo approach, which also allowed us to estimate the uncertainty of the fitting parameters in Table 6. Starting with a set of values for the fitting parameters in this table that resulted in a reasonable (eyeball) fit to the data, each of the values was randomly varied by up to ±50%, and were then used as a starting set of values in *fminsearch* to obtain a set of best fit values as described above. This entire process was repeated several hundred times. In some cases, a fit did not converge on a solution after 10,000 iterations of *fminsearch*; these fitting results were not used in subsequent calculations. Iterations that did converge to a solution were next examined, and those containing non-realistic best-fit values were also not considered further (i.e., negative rate constants or $\Delta^{14}C$ values lower than $-1000‰$). Finally, for the default model run (*run-A* in Section 4.3.2.1) all best fits whose *err* value was greater than 0.17 were removed. This threshold value was determined by an examination of a rank ordering of these results by increasing *err*. Fits that exceeded this threshold were likely obtained in solutions that found a "local" rather than a "global" minimum of *err*.

The results in Table 6 represent averages and standard deviations of the fitting parameters from fits that satisfied the criteria described above (on average this represented ~90 results, or about one half to one third of the total number of iterations). As the number of acceptable fits increased above ~30–40, there was no significant change in the resulting average values of the fitting parameters, although in some cases there was a slight decrease in their associated uncertainties. The results in Table 6 for *run-A* had an average value of *err* equal to 0.161 ± 0.004 (2% RSD), which can roughly be thought of as an average r^2 value of ~0.84 for the fit of the entire data set to the model.

4.3.2. Model results

We show results from two model runs: *run-A* that uses the default conditions described above, and *run-B* that includes an additional constraint on benthic DIC and DOC fluxes used in the estimation of *err*. It will be shown that the results of *run-A* fit the observed values well, but overestimated the amount of G_m inferred from the bulk POC profile. The cause for this discrepancy is explored through model *run-B*. We show that while the pool size and rate constant for G_{m1} differed significantly between *run-A* and *-B*, the overall results with regards to the reactivities and the isotopic compositions of the DOC pools were essentially identical.

4.3.2.1. run-A (default conditions). The best-fit model results for *run-A* are shown in Fig. 4a–l. The model captured the major trends in the data with reasonable accuracy including the sharp subsurface peaks in $\Delta^{14}C_{DOC}$ (Fig. 4h) and $\Delta^{14}C_{DIC}$ (Fig. 4k). The model predicted three isotopically distinct pools of metabolizable POC (Table 6 *run-A*; Fig. 6a): (1) G_{m1}, which contained bomb-^{14}C, and was abundant at the sediment–water interface but decayed rapidly within the top 3–4 cm; (2) G_{m2}, which did not show a bomb-^{14}C signal, but had a ~modern ^{14}C signature, and was sufficiently long-lived to persist throughout the top 20–25 cm of the sediment column; and (3) G_{m3}, which had similar reactivity as G_{m2}, but was much smaller in size, and was

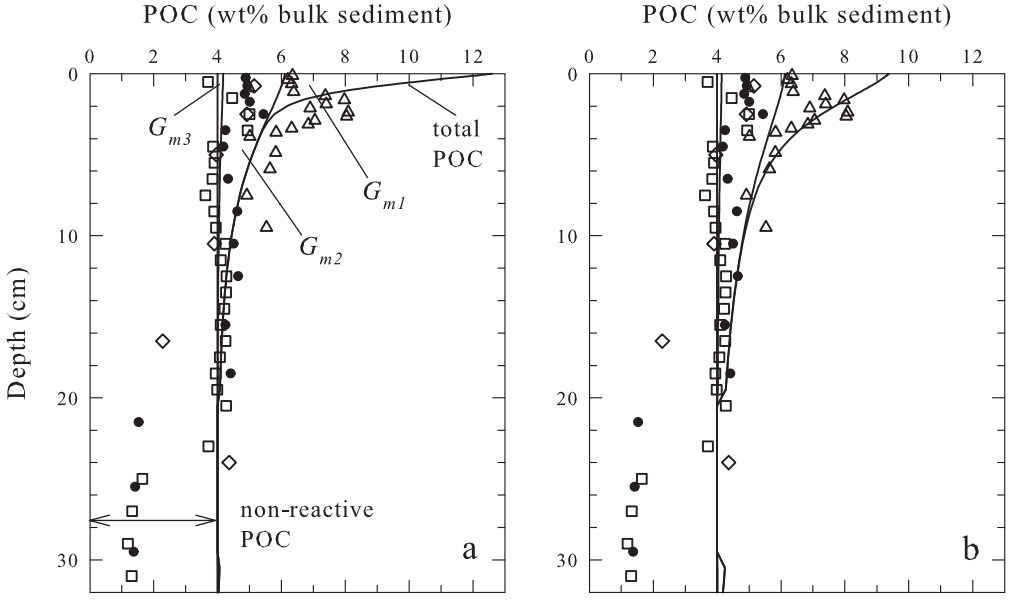

Fig. 6. Modeled G_m pools and observed bulk POC profiles for (a) model *run-A* (default conditions), and (b) model *run-B* (with benthic flux constraint). The four solid lines from left to right are: non-reactive POC (G_{nr}), $G_{nr} + G_{m3}$, $G_{nr} + G_{m3} + G_{m2}$, and G_{nr} + total G_m. G_{nr} is arbitrarily set at 4 wt.%. The model ignores the shift in POC across the 20 cm discontinuity. Symbols are bulk POC values measured at, and in close vicinity of, this site: triangles, Huh et al. (1987); diamonds, McManus et al. (2006); squares, Mollenhauer and Eglinton (2007); solid circles, this study.

Table 7
Summary of carbon degradation rates and fluxes.

	G_m			Depth-integrated degradation rate[a] (mmol m^{-2} d^{-1})	Benthic DOC flux (mmol m^{-2} d^{-1})	Benthic DIC flux (mmol m^{-2} d^{-1})	Fraction remineralized to DIC (%)
	Size (wt.% C)	$\delta^{13}C$ (‰)	$\Delta^{14}C$ (‰)				
Model run-A							
G_{m1}	6.5	−20.6	+48[−52][b]	1.99	1.11	0.88	44
G_{m2}	1.9	−22.2	−66	0.59	0.42	0.17	29
G_{m3}	0.18	−27	−520	0.05	0.05	0.00	<0.1
$J_{lb,DIC}$				0.32	0.00[c]	0.32	
Total	8.6(±0.9)	−21[c](±3)	+11[d](±21)	2.96	1.58	1.38	47
Model run-B							
G_{m1}	3.2	−18	+68[−58][b]	1.00	0.16	0.84	84
G_{m2}	2.0	−22.4	−45	0.58	0.33	0.25	43
G_{m3}	0.14	−26	−480	0.04	0.04	0.00	<0.1
$J_{lb,DIC}$				0.24	0.00[c]	0.24	
Total	5.4(±0.8)	−20[c](±4)	+12[d](±30)	1.86	0.52	1.33	72

[a] Rates corresponding to G_{mi} were calculated by integrating Eq. (A-5) over the model domain (0–45 cm) using parameters in Tables 5 and 6. Total rates are the sum of remineralization rates within the model domain and the diffusive flux of DIC from deeper sediments ($J_{lb,DIC}$).
[b] Pre-bomb value. See Appendix A for details.
[c] We assume there is no DOC flux from deeper sediments.
[d] Weighted average of the three G_m pools (post-bomb values were used for G_{m1}).

significantly depleted in both ^{14}C and ^{13}C. Degradation rate constants of G_m varied by an order of magnitude, from 0.1 yr^{-1} (k_1) to 0.7×10^{-2} yr^{-1} (k_2 and k_3), and were within the range of values expected for this type of sedimentary setting (Middelburg, 1989; Boudreau, 1997). As evident from Table 6 and Fig. 6a, the size of the combined G_m pool (8.6 wt.%) was greater than the observed core-top bulk POC content by a factor of ~2. The combined G_m pool was also a factor of ~7 greater than the observed decrease in bulk POC with depth (~1.5 wt.%; Fig. 6a). Possible explanations for this discrepancy are discussed in Section 4.3.3.

The model yielded degradation rate constants for DOC_1 DOC_2 and DOC_3 that varied by five orders of magnitude (Table 6). DOC_1 with a bomb-^{14}C signature was produced from rapid decay of G_{m1}, resulting in a sharp increase in DOC_1 concentration across the sediment–water interface (dashed lines in Fig. 4a and g). However, because of its high reactivity ($k_{DOC_1} = 33 \pm 9$ yr^{-1}), the concentration of DOC_1 peaked at ~1 cm depth, and was largely absent by 5 cm. In contrast, DOC_2 with a ~modern ^{14}C-signature was sufficiently long-lived to account for the majority of the DOC standing stock at all depths below ~1 cm ($k_{DOC_2} = 0.16 \pm 0.06$ yr^{-1}; dotted lines in Fig. 4a and g). The concentration of DOC_2 increased steadily with depth from the sediment–water interface to ca. 10 cm, then decreased as G_{m2} was gradually consumed (Fig. 6a). Although in the model we assumed identical values for k_2 and k_3, k_{DOC_3} was three orders of magnitude lower than k_{DOC_2}, rendering DOC_3 virtually non-reactive in these sediments. Because of the limited size of G_{m3} (Table 6), DOC_3 increased slowly with depth in the sediment, and accounted for ~50% of the bulk DOC content at 45 cm depth (dash-dot lines in Fig. 4a and g). Although DOC_3 was a minor component of the bulk DOC pool in most of the sediment column, given that its $\Delta^{14}C$ value was significantly depleted relative to those of DOC_1 and DOC_2 (−520‰ relative to +48‰ to −66‰; Table 6), the presence of DOC_3 was essential in reproducing the ~200‰ drop that was observed in $\Delta^{14}C_{DOC}$ with sediment depth (Fig. 4b and e).

The fit to the $\delta^{13}C_{DOC}$ data also captured the general trends in the data, but compared to $\Delta^{14}C$, there was greater variability in the measured values themselves. Nonetheless, the model predicted a $\delta^{13}C$ value for G_{m3} (−27‰) that was significantly lower than those for G_{m1} and G_{m2} (−21‰ to −22‰; Table 6). This suggests that G_{m3} may have been relatively enriched in terrestrial OC, and/or that it was enriched in lipids, which are in general depleted in ^{13}C compared to bulk POC (e.g., Hayes et al., 1990). $\delta^{13}C$ values ranging from ~−25‰ to as low as ~−43‰ have been reported for long-chain fatty acids and *n*-alkanes extracted from SMB sediments (Gong and Hollander, 1997; Pearson and Eglinton, 2000; Mollenhauer and Eglinton, 2007).

4.3.2.2. run-B (with benthic flux constraint). Although the model was able to capture the key features of the observed profiles with reasonable accuracy, the best-fit parameters from *run-A* predicted a combined G_m pool that significantly exceeded the total bulk POC observed in this study (Fig. 6a). The results of *run-A* also predicted a benthic DOC flux of 1.58 mmol m^{-2} d^{-1} which was comparable in magnitude to the benthic DIC flux (Table 7). This finding is inconsistent with previous studies that have shown benthic DOC fluxes to be generally smaller than benthic DIC fluxes in continental margin and coastal marine sediments (Alperin et al., 1999; Burdige et al., 1999). To address these inconsistencies, we employed the following relationship between benthic DOC and DIC fluxes reported for the continental margin (Burdige et al., 1999) as an additional fitting constraint in the model:

predicted benthic DOC flux

$$= 0.36 \times (\text{benthic DIC flux})^{0.29}. \quad (15)$$

To incorporate this constraint into the fitting process, at the end of each iteration we calculated the benthic DIC flux with the model data and Fick's First Law, then calculated the predicted benthic DOC flux using Eq. (15). An additional term used to calculate *err* was then determined as

$$\left|\frac{\text{predicted benthic DOC flux} - \text{modelled benthic DOC flux}}{\text{predicted benthic DOC flux}}\right| \quad (16)$$

where the modeled benthic DOC flux was similarly determined using model results and Fick's Law. This new error term was then averaged with the six $1 - r^2$ terms defined earlier (for DOC and DIC concentration, $\delta^{13}C$ and $\Delta^{14}C$ depth profiles; see Section 4.3.1) to obtain a new version of the parameter *err*.

The overall fit of this model *run-B* to the data is shown in Fig. 4m–x, and the best-fit parameters are shown in Table 6. Introduction of Eq. (15) as an additional constraint lowered the combined G_m pool by about one third, to 5.4 wt.% C, which in turn reduced the benthic DOC flux by approximately two thirds, while causing minimal change in the benthic DIC flux (Table 7). The ratio of the benthic DOC flux to the benthic DIC flux based on the results of *run-B* (0.39) was significantly lower than that in *run-A* (1.1), but still exceeded the value predicted by Eq. (15) by about 25%.

The drop in the size of the combined G_m pool in *run-B* relative to *run-A* was due to a reduction in the size of the G_{m1} pool (from 6.5 to 3.2 wt.% C); G_{m2} and G_{m3} pool sizes were largely unaffected. k_1 (and to a lesser extent, k_2) was also reduced, resulting in deeper penetration of G_{m1} into the sediments (Fig. 6). With the exception of δ_1 which was slightly heavier in *run-B*, all other fitting parameters were within error of, or close to, those from *run-A* (Table 6).

Model *run-B* fit the data as well as *run-A* in most respects (Fig. 4). However, a key difference was that with the attenuation of ^{14}C-rich G_{m1} and its degradation rate constant, the prominent subsurface maximum in $\Delta^{14}C_{DOC}$ was no longer captured (Fig. 4t). Furthermore, the discrepancy between observed POC and modeled G_m remained unresolved; the combined G_m pool in *run-B* exceeded the down-core decrease in POC by a factor of 3.6 (Fig. 6).

4.3.3. Reconciling model results and observed data

Although the selective degradation model fit the observed data reasonably well (Fig. 4), both *run-A* and *run-B* predicted the presence of large pools of G_m that are similar in size to, or exceed the total amount of POC observed in the core-top (Fig. 6). In addition, the predicted benthic DOC flux was higher than expected (especially in *run-A*), and adding the benthic DOC flux constraint in *run-B* resulted in an underestimation of the $\Delta^{14}C_{DOC}$ peak present within the uppermost 3 cm of the sediment column. In this section, we discuss possible causes for the discrepancy between modeled and measured values of POC and DOC fluxes.

The lack of agreement between the modeled and observed amount of metabolizable POC could, in part, be explained by spatial variability in POC in these sediments, combined with the fact that POC and DOC samples were obtained from different multicore casts (Tables 2 and 3). Comparison of bulk POC profiles from four studies conducted in this region of the SMB show considerable scatter within the 0–10 cm interval; core-top POC varies by almost a factor of two, from <4 to >6 wt.% (Fig. 6). The cause for spatial variability in POC is unclear. Despite this core-top variability, the four data sets converge below ~10 cm depth. These observations are consistent with a patchy distribution of metabolizable POC in this region of the SMB. Non-uniform distribution of labile POC could cause a discrepancy between the occurrence of labile DOC (derived from G_{m1}) and bulk POC, because DOC is subject to molecular diffusion while POC is not.

In addition, Huh et al. (1987) provide evidence for sediment mixing in the uppermost 1–2 cm of these sediments. If labile organic floc on the seafloor is mixed into the uppermost few cm of the sediment column and is subsequently solubilized, it could result in an increase in DOC and $\Delta^{14}C_{DOC}$ with little to no change in the bulk POC profile. Consistent with this suggestion are simple calculations presented in Burdige (2006), which show that for a fixed carbon rain rate to the sediments, the surface POC concentration decreases as bioturbation coefficients increase. Furthermore, the carbon content of sinking POC in the center of the SMB ranges from 5 to 20 wt.% (Williams et al., 1992) providing a possible mechanism for adding organic-rich material to the surface sediments.

The occurrence of sediment mixing is nonetheless puzzling given the low dissolved oxygen concentrations in the central floor of the SMB, and the observed lamination of these sediments. Huh et al. (1987) suspected bottom currents and artificial mixing during core recovery and processing. Alternatively, Prokopenko et al. (2011) and Chong et al. (2012) provide strong evidence for biological transport of bottom-water NO_3^- into these sediments to 2–3 cm depth. In light of these data, we propose that the disagreement between the model-predicted and observed pool sizes of metabolizable POC may be due to some combination of patchy POC distribution and physical mixing in the top ~2 cm of the sediment column.

A possible explanation for the elevated model-derived benthic DOC flux begins with the observation that the sum of the model-derived benthic DOC and DIC fluxes (1.9 [*run-B*] to 3.0 [*run-A*] mmol m^{-2} d^{-1}; Table 7) agree well with directly determined depth-integrated rates of carbon oxidation reported previously for SMB sediments (1.7–2.7 mmol m^{-2} d^{-1}; Jahnke, 1990; Berelson et al., 1996). This then suggests the possibility that for a fixed POC rain rate to the sediments, the current model fails to adequately partition the net flow of carbon to DOC versus DIC, such that it overestimates the benthic DOC flux. For example, this can be envisioned if there is enhanced remineralization of DOC from G_{m1} (and perhaps from G_{m2}) near the sediment surface that is not observable with the ~0.25 cm resolution of our pore water sampling. The overall effect would be to overestimate the pore-water DOC gradient

and hence the benthic DOC flux, and underestimate the benthic DIC flux, leading to the observed discrepancy between the model-derived DOC:DIC benthic flux ratio and that predicted by Eq. (15).

It is also possible that the benthic DOC flux was overestimated due to an incorrect choice of the DOC diffusion coefficient used in our model (D_o^{DOC}; Table 5). Because pore-water DOC is poorly characterized on several levels, the value of D_o^{DOC} used here was based on an empirical log–log relationship between DOC diffusion coefficients and molecular weights, and the assumption that the log-average molecular weight of pore-water DOC is 1.6 kDa (Burdige et al., 1992; Alperin et al., 1994). Therefore, the model will overestimate the benthic DOC flux if pore-water DOC near the sediment–water interface in SMB sediments was dominated by significantly larger molecules. Indeed, if D_o^{DOC} is decreased to ~30% of the default value (14 $cm^2\ yr^{-1}$ as opposed to 50 $cm^2\ yr^{-1}$), it is possible to obtain a model fit to the data that is essentially identical that of *run-A* shown in Fig. 4, and at the same time obtain a benthic DOC flux that satisfies Eq. (15). However, this D_o^{DOC} corresponds to a log-average molecular weight of 50 kDa for DOC in these sediments, which is significantly larger than what has been observed previously in marine sediments, including past studies of DOC in SMB sediments (Chin and Gschwend, 1991; Burdige and Gardner, 1998). Hence this explanation will hold only if the DOC encountered in this current study of SMB sediments was distinct in terms of size relative to what was observed previously. Furthermore, the discrepancy between modeled and observed POC is not resolved with this lower D_o^{DOC}; the model-derived value for the total G_m pool remained high at 5.5 wt.%. More work is needed to critically examine these possibilities.

4.3.4. Inferred composition and fate of metabolizable POC

Degradation of metabolizable POC and its fate as predicted by our model are summarized in Table 7. Regardless of model run, what appears to be contemporary OC of marine origin (G_{m1} and G_{m2}) dominated the metabolizable POC fraction. This is consistent with the widely reported preferential loss of ^{14}C-enriched OC during chemical and biological degradation of POC (e.g., Cherrier et al. 1999; Aller and Blair 2004; Purinton et al. 2008). Of the DOC generated from G_{m1} and G_{m2}, significant fractions (40–80% and 30–40%, respectively) were oxidized to DIC within the sediments, while the remainder diffused out to the water column as DOC. Because G_{m1} and G_{m2} together constituted $\geqslant$97% of metabolizable POC, the isotopic compositions of pore-water DIC and DOC (and hence the isotopic composition of the benthic DIC and DOC fluxes) were largely determined by those of G_{m1} and G_{m2}. In contrast, remineralization of the least reactive G_{m3} pool contributed very little to sediment DIC production because of its small size and the low reactivity of DOC_3. Unlike DOC_1 and DOC_2 that were partially oxidized in the pore waters, virtually all DOC_3 remained intact in the sediments. DOC_3 supported only ~3–8% of the benthic DOC flux, but because $k_{DOC_3} \ll k_{DOC_2}$ and k_{DOC_1} (Table 6), DOC_3 could have a greater influence on the concentration and isotopic values of bottom-water DOC than DOC_1 and DOC_2.

As a means of evaluating the model output, we compared the isotopic values of G_m to measured isotopic values of POC compound classes. The model-derived $\Delta^{14}C$ values of G_{m1}, G_{m2} and G_{m3} (+68‰ to −520‰; Table 6) broadly overlapped with the range of $\Delta^{14}C$ values observed for AS_{calc}, AI and TL fractions (+38‰ to −773‰; Table 2). The $\delta^{13}C$ values of G_{m1} and G_{m2} were marine-like, and were similar to those of the AS_{calc} fraction and bulk POC, respectively (Fig. 2c, Table 6). In addition, the $\Delta^{14}C$ value of G_{m1} was similar to those of the AS_{calc} fraction. The similarity in isotopic composition between model-derived labile fractions of bulk POC and those determined by selective extraction techniques lends support to our model calculations. The $\delta^{13}C$ value of G_{m3} was depleted relative to all organic fractions examined, but was within range of $\delta^{13}C$ values reported for short- and long-chain fatty acids extracted from this site (see Section 4.3.2.1, Fig. 2c, and Table 6; also see Gong and Hollander, 1997; Mollenhauer and Eglinton, 2007).

To further evaluate the model output, we used our results to calculate the carbon content and isotopic values of POC supplied to these sediments, and compared them to values available in the literature. In this calculation, it was assumed that the amount of POC supplied to the sediments is equal to the sum of POC buried (approximated by values in the 18–19 cm depth interval) and POC that was subject to degradation in the surface sediments as predicted by the model (Table 7). In addition, as was done in our selective degradation model, we ignored any DOC production occurring in sediments deeper than 45 cm (Fig. 3). If DOC production continued well below 45 cm, and ^{14}C-depleted DOC was supplied into the surface sediments by upward diffusion, our predicted $\Delta^{14}C$ signature of POC supplied to these sediments would likely be an underestimate. For *run-A*, this approach gave the following values for wt.% OC, $\delta^{13}C$, and $\Delta^{14}C$: 13 ± 1 wt.%, -21 ± 3‰, and -60 ± 15‰, respectively. *run-B* gave the same $\delta^{13}C$ value and an overlapping $\Delta^{14}C$ value (-84 ± 19‰), but the POC content was somewhat lower (9.4 ± 0.8 wt.%). The carbon content and $\delta^{13}C$ signature estimated here agreed well with those of sinking POC captured at 850 m in the center of the basin (5–20 wt.% POC; −22.4‰ to −21.1‰; Williams et al., 1992). The calculated $\Delta^{14}C$ values were lower than those reported for sinking POC at 850 m (~+40‰; Williams et al., 1992), although this is expected given that the sediment trap data were collected in the mid- to late-1980s when surface-ocean $\Delta^{14}C_{DIC}$ values were higher (Pearson et al., 2001), and as discussed in Section 4.1, this site also receives pre-aged POC through lateral transport. Our calculated $\Delta^{14}C$ values were closer to a model-derived $\Delta^{14}C$ signature of POC supplied to a nearby 100-m shelf site (-160 ± 60‰; Hwang et al., 2005).

4.4. Benthic DOC dynamics and their potential role in the marine OC cycle

Our model results suggest that sedimentary POC degradation can be minimally described as a two-step process in which POC, regardless of its inherent reactivity, is initially degraded to a pool of DOC intermediates that may then

be degraded to DIC. The presence of ^{14}C-depleted, refractory DOC in the pore water (DOC_3) further suggest that POC degradation is not limited to young and labile OC, and that some old, inherently refractory POC is also decomposed (i.e., these results support pathway (b) in Fig. 1). Degradation of pre-aged, resistant POC is consistent with the apparent efficiency with which terrestrial POC (which survived oxidation on land) is lost in the marine environment (Burdige 2005; Bianchi, 2011; Blair and Aller, 2012), and is also consistent with net accumulation of ^{14}C-depleted DOC observed in an incubation experiment (Komada et al., 2012). One implication from the present study is that once this refractory POC is degraded, it may evade complete oxidation to DIC and accumulate in the DOC pool, at least within anoxic sediments.

As was done in our model, conceptual and quantitative models of DOC cycling in the marine water column have been used to define DOC fractions based on their inferred reactivity (Carlson, 2002; Hansell et al., 2012). These fractions are referred to as "labile" DOC (lifetime <1 yr), semi-labile DOC (lifetime ~1–2 yrs), semi-refractory DOC (lifetime ~20 yrs) and refractory DOC (lifetime ~16,000 yrs). For comparison, the degradation rate constants for the three DOC fractions in our model can be expressed in terms of DOC lifetimes ($\tau = 1/k$). In this format, DOC_1 has a lifetime of ~0.01–0.03 yr, while DOC_2 has a lifetime of ~4–6 yrs, and DOC_3 has a lifetime $>10^3$ yrs. Based on this comparison of lifetimes, the reactivity of DOC_1 and DOC_3 are similar to those of labile and refractory DOC in the water column models, respectively, while the reactivity of DOC_2 falls somewhere between those of semi-labile and semi-refractory DOC.

Our model findings further suggest that pore-water DOC at any given instance is a mixture of components of varying reactivities and isotopic signatures (Table 7). On average, pore-water DOC near the sediment surface appears ^{14}C-young and labile, and upon escaping the sediments as a benthic flux, the majority of this material is likely to be rapidly oxidized in the water column. This conclusion is consistent with the above comparison of our results to analogous modeling studies of water column DOC distributions, as well as with previous findings from this site and the continental rise of the North Pacific Ocean (Bauer et al., 1995). However, our analysis strongly suggests the presence of an aged, refractory DOC component as well. The fate of this refractory component in the water column is unclear. It could be efficiently removed due to the higher redox potential in the water column, or could be removed by processes such as photochemical degradation (Mopper and Kieber, 2002) or incorporation into POC (Druffel and Williams, 1990; Hwang et al. 2006). Alternatively, some fraction of the refractory pore-water DOC could persist in the water column, because studies on microbial extracellular enzyme activities show lower and less versatile activities in the water column relative to underlying sediments (Arnosti, 2010 and references therein).

On a global scale, benthic DOC fluxes from coastal and continental margin sediments have been estimated to amount to ~180 Tg C yr^{-1} (Burdige et al., 1999). As a first-order assessment, if we assume that these fluxes are compositionally similar to that found in this study (Table 7), then 3–8% (or 5–14 Tg C yr^{-1}) of DOC fluxes from coastal and continental margin sediments could consist of materials similar in nature to DOC_3. These fluxes represent 12–33% of the turnover rate of refractory DOC in the deep ocean determined by modeling DOC distributions in the global oceans (43 Tg C yr^{-1}; Hansell et al., 2012). Further work is needed to better constrain the production rate of refractory pore-water DOC in sediments, its fate in the marine water column, and the role it plays in determining the Δ^{14}C of deep ocean DOC.

ACKNOWLEDGEMENTS

We thank Amy Pitts, Jonathon Polly, Malee Jinuntuya, Raman Paul, Jim Fuller, the Captain and crew of R/V Point Sur, and the late Nuria Protopopescu for their assistance in this project. We also thank Hans Jannasch for lending us his gimbal stand, Gesine Mollenhauer for sharing SMB-900 POC data, Xiaomei Xu for her relentless help with AMS measurements, and Steve Beaupré and Will Berelson for helpful discussions. Comments from 4 anonymous reviewers helped improve the quality of the first version of this manuscript. DL was supported by a scholarship from the NSF (NSF REU 05-569). This work was supported by Grants from the NSF (OCE-0726819 to T.K., OCE-0727179 to D.B.).

APPENDIX A. SOLUTIONS TO THE MODEL EQUATIONS

Solute. equations

Variations with depth in sediment porosity due to either sediment compaction or turbidite emplacement impact solute diffusion in sediments. This occurs because the bulk sediment diffusion coefficient of a solute (expressed here simply as D_s) is related to the solute's free solution diffusion coefficient ($D°$) by the equation $D_s = D^0/\theta^2$, where θ^2, the sediment tortuosity, is generally expressed as a function of sediment porosity (e.g., Boudreau and Meysman, 2006). Here we express this porosity dependency with the modified Weissberg relationship $\theta^2 = 1 - 2\ln(\varphi)$ (Boudreau, 1997), and as a result, the diffusive terms in the DOC and DIC model equations in Table 4 are expanded as follows (note that here C is taken as either solute),

$$\frac{1}{\varphi}\frac{\partial}{\partial x}\left(\varphi D_s \frac{\partial C}{\partial x}\right) = \frac{D^o}{\varphi}\frac{\partial}{\partial x}\left(\frac{\varphi}{\theta^2}\frac{\partial C}{\partial x}\right) = \frac{D^o}{\theta^2}\frac{\partial^2 C}{\partial x^2} + \frac{D^o}{\varphi}\frac{d\psi}{dx}\frac{\partial C}{\partial x} \quad \text{(A-1)}$$

where

$$\psi = \frac{\varphi}{\theta^2} \quad \text{(A-2)}$$

and

$$\frac{d\psi}{dx} = \frac{d\varphi}{dx}\left[\frac{3 - 2\ln(\varphi)}{[1 - 2\ln(\varphi)]^2}\right]. \quad \text{(A-3)}$$

The depth dependences of φ and $\frac{d\varphi}{dx}$ (as discussed in the text and in Eqs. (13) and (14)) were used to define $\frac{d\psi}{dx}$ in the

numerical solutions to the DOC and DIC model equations in Table 4.

Solid. phase equations

In this discussion we initially neglect the emplacement of a turbidite in the sediment column we are modeling, and note that sedimentation between turbidite layers appears to have remained steady over the last ~7000 yrs (Romans et al. 2009). In this case, a generic form of the reactive transport equation for a G_m fraction in sediments in which porosity simply varies with depth due to sediment compaction is given by

$$\frac{1}{(1-\varphi)}\frac{\partial}{\partial x}(\omega(1-\varphi)G_{mi}) - k_i G_{mi} = 0 \tag{A-4}$$

where ω is the sediment accumulation rate, and all other parameters are defined in the text. If the mass flux to the sediments (W) is constant with depth (and time), then conservation of mass and pore water implies that $(1-\varphi)\omega = W/\rho_{ds}$ (Meysman et al., 2005; Burdige, 2006), where ρ_{ds}, the dry sediment density is also assumed to be constant with depth. With this, Eq. (A-4) can be re-written as,

$$\frac{W}{(1-\varphi)\rho_{ds}}\frac{\partial G_{mi}}{\partial x} - k_i G_{mi} = 0. \tag{A-5}$$

Using Eq. (13) to define the depth dependence of porosity, the first derivative in Eq. (A-5) was approximated using a backwards differencing scheme. An uneven grid was used from 0 to 45 cm (the model domain) in which Δx increased from 0.005–1 cm as a function of depth, to better capture the finer details of the profiles near the sediment–water interface. The resulting numerical approximation of Eq. (A-5) was solved as discussed in Boudreau (1997; see Eq. 8.49). The boundary condition for each of these model equations specifies the concentration G^o_{mi} at $x = 0$ (the sediment–water interface).

For the G_{m1} fraction, degradation of this material is complete above the top of the turbidite. The numerical solution described above was therefore used to determine the depth distribution of this material, and hence to define the depth distribution of DOC_1 production ($=k_1 G_{m1}$) in the pore water DOC equations in Table 4. In contrast, the depth/time scales over which G_{m2} and G_{m3} are remineralized implies that deposition of this turbidite will "interrupt" the depth distribution of G_{m2} and G_{m3} remineralization. To account for this, we assume that the deposition of this turbidite was an instantaneous process (Romans et al., 2009) and that the turbidite contains no G_{m2}- or G_{m3}-type POC. Furthermore, if we refer to the G_{mi} profile that results from the solution to Eq. (A-5) as G^{sol}_{mi} then we can approximate the "true" G_{m2} and G_{m3} profile today as

$$G_{mi}(x) = \begin{cases} G^{sol}_{mi}(x) & (x < zt_{top}) \\ 0 & (zt_{bot} \geqslant x \geqslant zt_{top}) \\ G^{sol}_{mi}(x - tt) & (x > zt_{bot}) \end{cases} \tag{A-6}$$

where $tt = zt_{top} - zt_{bot}$. Again, these profiles of G_{m2} and G_{m3} were used to define the depth distribution of DOC_2 and DOC_3 production. Since porosity changes slowly below ~5–10 cm sediment depth (with the exception of sediments within the turbidite) the effects of sediment compaction on solid phase sediment profiles become less important at depth, and as a result this approach appears to be a reasonable approximation for the instantaneous G_{mi} profiles in SMB sediments.

The depth distributions of G^{13}_{mi} used for the $DO^{13}C_i$ production terms in Eq. (6) were calculated from the G_{mi} distributions determined above as:

$$G^{13}_{mi} = G_{mi} \cdot r^{13}_{G_{mi}} \tag{A-7}$$

where r^{13}_i, the fractional abundance of ^{13}C in species i is:

$$r^{13}_i = \left(\frac{^{13}C}{C}\right)_i = \left[1 + \frac{1000}{(\delta^{13}C_i + 1000)R_{PDB}}\right]^{-1} \tag{A-8}$$

The depth distributions of G^{14}_{mi} used for the $DO^{14}C_i$ production terms in Eq. (7) were determined by numerically solving (as described above) a version of Eq. (A-5) that also accounts for radioactive decay,

$$\frac{W}{(1-\varphi)\rho_{ds}}\frac{\partial G^{14}_{mi}}{\partial x} - (k_i + \lambda)G^{14}_{mi} = 0 \tag{A-9}$$

and then, for G^{14}_{m2} and G^{14}_{m3}, modifying these solutions to account for turbidite emplacement using Eq. (A-6). The boundary condition of each of these model equations specifies the concentration of G^{14}_{mi} at $x = 0$ according to:

$$G^{14}_{mi} = G^{12}_{mi} \cdot r^{14}_{G_{mi}} \tag{A-10}$$

where r^{14}_i is given by:

$$r^{14}_i = \left(\frac{^{13}C}{^{12}C}\right)_i = F_{mi} \cdot R_{abs} \cdot \left\{\frac{1 + 0.001 \cdot (-25)}{1 + 0.001 \cdot \delta^{13}C}\right\}^{-2} \tag{A-11}$$

and F_{mi}, the fraction modern (F_m) value of species i, is related to the value of $\Delta^{14}C$ of species i by Eq. (12). To simulate the pore-water ^{14}C gradients as accurately as possible, r^{14}_i values in Eq. (A-11) were determined from F_{mj} after removing the $\delta^{13}C$ normalization (Mook and van der Plicht, 1999).

Finally, deposition of POC to these sediments has an additional temporal component, because surface-water derived POC deposited to the sediments after ~1960 (corresponding to the uppermost ~2 cm of the sediment column) contains bomb-^{14}C (McNichol and Aluwuihare, 2007). We assume here that this phenomenon only affects the G_{m1} pool. We make this assumption because the depth scales over which the G_{m2} and G_{m3} pools are degraded are such that the vast majority of these pools that is currently undergoing degradation in SMB sediments is pre-1960 material (Fig. 6).

In contrast, significant degradation of G_{m1}, occurs both above and below the bomb horizon. Because bioturbation is virtually absent in SMB sediments, we simply assumed that G_{m1} present at depths greater than 2 cm is free of bomb-^{14}C signature (i.e., Δ_{1pre} in Table 6) while G_{m1} in shallower sediments contain bomb-^{14}C (Δ_1 in Table 6). As a result, the value of r^{14}_{Gm1} used in Eq. (A-10) and ultimately in the solution to Eq. (A-9) differ above and below this 2 cm sediment horizon (Δ_1 for sediments above 2 cm and Δ_{1pre} for deeper sediments).

REFERENCES

Aller R. C. and Blair N. E. (2004) Early diagenetic remineralization of sedimentary organic C in the Gulf of Papua deltaic complex (Papua New Guinea): net loss of terrestrial C and diagenetic fractionation of C isotopes. *Geochim. Cosmochim. Acta* **68**, 1815–1825.

Aller R. C. and Blair N. E. (2006) Carbon remineralization in the Amazon-Guianas tropical mobile budbelt: a sedimentary incinerator. *Cont. Shelf Res.* **26**, 2241–2259.

Alperin M. J. and Martens C. S. (1993) Dissolved organic carbon in marine pore waters: a comparison of three oxidation methods. *Mar. Chem.* **41**, 135–143.

Alperin M. J., Albert D. B. and Martens C. S. (1994) Seasonal variations in production and consumption rates of dissolved organic carbon in an organic-rich coastal sediment. *Geochim. Cosmochim. Acta* **58**, 4909–4930.

Alperin M. J., Martens C. S., Albert D. B., Suayah I. B., Benninger L. K., Blair N. E. and Jahnke R. A. (1999) Benthic fluxes and porewater concentration profiles of dissolved organic carbon in sediments from the North Carolina continental slope. *Geochim. Cosmochim. Acta* **63**, 427–448.

Amon R. M. W. and Benner R. (1996) Bacterial utilization of different size classes of dissolved organic matter. *Limnol. Oceanogr.* **41**, 41–51.

Arnosti C. (2010) Microbial extracellular enzymes and the marine carbon cycle. *Annu. Rev. Mar. Sci.* **3**, 401–425.

Bauer J. E., Reimers C. E., Druffel E. R. M. and Williams P. M. (1995) Isotopic constraints on carbon exchange between deep ocean sediments and sea water. *Nature* **373**, 686–689.

Beaupré S. R., Druffel E. R. M. and Griffin S. (2007) A low-blank photochemical extraction system for concentration and isotopic analyses of marine dissolved organic carbon. *Limnol. Oceanogr. Methods* **5**, 174–184.

Berelson W. M. and Stott L. D. (2003) Productivity and organic carbon rain to the California margin seafloor: modern and paleoceanographic perspectives. *Paleoceanography* **18**. http://dx.doi.org/10.1029/2001PA000672.

Berelson W. M., McManus J., Coale K. H., Johnson K. S., Kilgore T., Burdige D. J. and Pilskaln C. (1996) Biogenic matter diagenesis on the sea floor: a comparison between two continental margin transects. *J. Mar. Res.* **54**, 731–762.

Bianchi T. S. (2011) The role of terrestrially derived organic carbon in the coastal ocean: a changing paradigm and the priming effect. *Proc. Natl. Acad. Sci. USA* **108**, 19473–19481.

Blair N. E. and Aller R. C. (2012) The fate of terrestrial organic carbon in the marine environment. *Annu. Rev. Mar. Sci.* **4**, 401–423.

Boehme S. E., Blair N. E., Chanton J. P. and Martens C. A. (1996) A mass balance of ^{13}C and ^{12}C in an organic-rich methane-producing marine sediment. *Geochim. Cosmochim. Acta* **60**, 3835–3848.

Boudreau B. P. (1997) *Diagenetic Models and Their Implementation*. Springer-Verlag.

Boudreau B. P. and Meysman F. J. R. (2006) Predicted tortuosity of muds. *Geology* **34**, 693–696.

Burdige D. J. (2001) Dissolved organic matter in Chesapeake Bay sediment pore waters. *Org. Geochem.* **32**, 487–505.

Burdige D. J. (2002) Sediment pore waters. In *Biogeochemistry of Marine Dissolved Organic Matter* (eds. D. A. Hansell and C. A. Carlson). Academic Press, p. 774.

Burdige D. J. (2005) Burial of terrestrial organic matter in marine sediments: a re-assessment. *Global Biogeochem. Cycles* **19**, GB4011. http://dx.doi.org/10.1029/2004GB002368.

Burdige D. J. (2006) *Geochemistry of Marine Sediments*. Princeton University Press.

Burdige D. J. (2007) Preservation of organic matter in marine sediments: controls, mechanisms, and an imbalance in sediment organic carbon budgets? *Chem. Rev.* **107**, 467–485.

Burdige D. J. and Gardner K. G. (1998) Molecular weight distribution of dissolved organic carbon in marine sediment pore waters. *Mar. Chem.* **62**, 45–64.

Burdige D. J. and Komada T. (2011) Anaerobic oxidation of methane and the stoichiometry of remineralization processes in continental margin sediments. *Limnol. Oceanogr.* **56**, 1781–1796.

Burdige D. J. and Martens C. S. (1990) Biogeochemical cycling in an organic-rich coastal marine basin: 11. The sedimentary cycling of dissolved, free amino acids. *Geochim. Cosmochim. Acta* **54**, 3033–3051.

Burdige D. J., Alperin M. J., Homstead J. and Martens C. S. (1992) The role of benthic fluxes of dissolved organic carbon in oceanic and sedimentary carbon cycling. *Geophys. Res. Lett.* **19**, 1851–1854.

Burdige D. J., Berelson W. M., Coale K. H., McManus J. and Johnson K. S. (1999) Fluxes of dissolved organic carbon from California continental margin sediments. *Geochim. Cosmochim. Acta* **63**, 1507–1515.

Burdige D. J., Skoog A. and Gardner K. (2000) Dissolved and particulate carbohydrates in contrasting marine sediments. *Geochim. Cosmochim. Acta* **64**, 1029–1041.

Carlson C. A. (2002) Production and removal processes. In *Biogeochemistry of Marine Dissolved Organic Matter* (ed. D. A. Hansell and C. A. Carlson). Academic Press, San Diego.

Cherrier J., Bauer J. E., Druffel E. R. M., Coffin R. B. and Chanton J. P. (1999) Radiocarbon in marine bacteria: evidence for the ages of assimilated carbon. *Limnol. Oceanogr.* **44**, 730–736.

Chin Y.-P. and Gschwend P. M. (1991) The abundance, distribution, and configuration of porewater organic colloids in recent sediments. *Geochim. Cosmochim. Acta* **55**, 1309–1317.

Chong L. S., Prokopenko M. G., Berelson W. M., Townsend-Small A. and McManus J. (2012) Nitrogen cycling within suboxic and anoxic sediments from the continental margin of Western North America. *Mar. Chem.* **128–120**, 13–25.

Christensen C. J., Gorsline D. S., Hammond D. E. and Lund S. P. (1994) Non-annual laminations and expansion of anoxic basin-floor conditions in Santa Monica Basin, California Borderland, over the past four centuries. *Mar. Geol.* **116**, 399–418.

Degens E. T., Behrendt M., Gotthardt B. and Reppmann E. (1968) Metabolic fractionation of carbon isotopes in marine plankton-II. Data on samples collected off the coasts of Peru and Ecuador. *Deep-Sea Res.* **15**, 11–20.

DeNiro M. and Epstein S. (1977) Mechanism of carbon isotope fractionation associated with lipid synthesis. *Science* **197**, 261–263.

DOE (1994) Handbook of methods for the analysis of the various parameters of the carbon dioxide system in sea water (eds. A. G. Dickson and C. Goyet). ORNL/CDIAC-74.

Drenzek N. J., Hughen K. A., Montlucon D. B., Southon J. R., dos Santos G. M., Druffel E. R. M., Giosan L. and Eglinton T. I. (2009) A new look at old carbon in active margin sediments. *Geology* **37**, 239–242.

Druffel E. R. M. and Williams P. M. (1990) Identification of a deep marine source of particulate organic carbon using bomb ^{14}C. *Nature* **347**, 172–174.

Druffel E. R. M., Williams P. M., Bauer J. E. and Ertel J. R. (1992) Cycling of dissolved and particulate organic matter in the open ocean. *J. Geophys. Res.* **97**(C10), 15639–15659.

Fenchel T., Blackburn T. H. and King G. (1998) *Bacterial Biogeochemistry: The Ecophysiology of Mineral Cycling*. Academic Press.

Gong C. and Hollander D. J. (1997) Differential contribution of bacteria to sedimentary organic matter in oxic and anoxic environments, Santa Monica Basin, California. *Org. Geochem.* **26**, 545–563.

Gorsline D. S. (1992) The geologic setting of Santa Monica and San Pedro Basins, California Continental Borderland. *Prog. Oceanogr.* **30**, 1–36.

Gorsline D. S. (1996) Depositional events in Santa Monica Basin, California Borderland, over the past five centuries. *Sediment. Geol.* **104**, 73–88.

Gorsline D. S., De Diego T. and Nava-Sanchez E. H. (2000) Seismically triggered turbidites in small margin basins: Alfonso Basin, Western Gulf of California and Santa Monica Basin, California Borderland. *Sediment. Geol.* **135**, 21–35.

Hansell D. A., Carlson C. A. and Schlitzer R. (2012) Net removal of major marine dissolved organic carbon fractions in the subsurface ocean. *Global Biogeochem. Cycles* **26**. http://dx.doi.org/10.1029/2011GB004069.

Hayes J. M., Freeman K. H., Popp B. N. and Hoham C. H. (1990) Compound-specific isotopic analysis: a novel tool for reconstruction of ancient biogeochemical processes. *Org. Geochem.* **16**, 1115–1128.

Hedges J. I. and Keil R. G. (1995) Sedimentary organic matter preservation: an assessment and speculative synthesis. *Mar. Chem.* **49**, 81–115.

Hee C. A., Pease T. K., Alperin M. J. and Martens C. S. (2001) Dissolved organic carbon production and consumption in anoxic marine sediments: a pulsed-tracer experiment. *Limnol. Oceanogr.* **46**, 1908–1920.

Huh C.-A., Zahnle D. L. and Small L. F. (1987) Budgets and behaviors of uranium and thorium series isotopes in Santa Monica Basin sediments. *Geochim. Cosmochim. Acta* **51**, 1743–1754.

Huh C.-A., Small L. F., Niemnil S., Finney B. P., Hickey B. M., Kachel N. B., Gorsline D. S. and Williams P. M. (1990) Sedimentation dynamics in the Santa Monica-San Pedro Basin off Los Angeles: radiochemical, sediment trap and transmissometer studies. *Cont. Shelf Res.* **10**, 137–164.

Hwang J. and Druffel E. R. M. (2005) Blank correction for $\Delta^{14}C$ measurements in organic compound classes of oceanic particulate matter. *Radiocarbon* **47**, 75–87.

Hwang J., Druffel E. R. M. and Komada T. (2005) Transport of organic carbon from the California coast to the slope region: A study of $\Delta^{14}C$ and $\delta^{13}C$ signatures of organic compound classes. *Global Biogeochem. Cycles* **19**. http://dx.doi.org/10.1029/2004GB002422.

Hwang J., Druffel E. R. M. and Bauer J. E. (2006) Incorporation of aged dissolved organic carbon (DOC) by oceanic particulate organic carbon (POC): an experimental approach using natural carbon isotopes. *Mar. Chem.* **98**, 315–322.

Ingram B. L. and Southon J. R. (1996) Reservoir ages in eastern Pacific coastal and estuarine waters. *Radiocarbon* **38**, 573–582.

Jahnke R. A. (1990) Early diagenesis and recycling of biogenic debris at the seafloor, Santa Monica Basin, California. *J. Mar. Res.* **48**, 413–436.

Johnson L. and Komada T. (2011) Determination of radiocarbon in marine sediment porewater dissolved organic carbon by thermal sulfate reduction. *Limnol. Oceanogr. Meth.* **9**, 485–498.

Koch B. P., Witt M., Engbrodt R., Dittmar T. and Kattner G. (2005) Molecular formulae of marine and terrigenous dissolved organic matter detected by electrospray ionization Fourier transform ion cyclotron resonance mass spectrometry. *Geochim. Cosmochim. Acta* **69**, 3299–3308.

Komada T., Reimers C. E., Luther, III, G. W. and Burdige D. J. (2004) Factors affecting dissolved organic matter dynamics in mixed-redox to anoxic coastal sediments. *Geochim. Cosmochim. Acta* **68**, 4099–4111.

Komada T., Druffel E. R. M. and Hwang J. (2005) Sedimentary rocks as sources of ancient organic carbon to the ocean: an investigation through $\Delta^{14}C$ and $\delta^{13}C$ signatures of organic compound classes. *Global Biogeochem. Cycles* **19**, GB2017. http://dx.doi.org/10.1029/2004GB002347.

Komada T., Anderson M. R. and Dorfmeier C. L. (2008) Carbonate removal from coastal sediments for the determination of organic carbon and its isotopic signatures, $\delta^{13}C$ and $\Delta^{14}C$: comparison of fumigation and direct acidification by hydrochloric acid. *Limnol. Oceanogr. Meth.* **6**, 254–262.

Komada T., Polly J. A. and Johnson L. (2012) Transformations of carbon in anoxic marine sediments: Implications from $\Delta^{14}C$ and $\delta^{13}C$ signatures. *Limnol. Oceanogr.* **57**, 567–581.

Lomstein B. A., Jensen A.-G. U., Hansen J. W., Andreasen J. B., Hansen L. S., Berntsen J. and Kunzerdorf H. (1998) Budgets of sediment nitrogen and carbon cycling in the shallow water of Knebel Vig, Denmark. *Aquat. Microb. Ecol.* **14**, 69–80.

Masiello C. A. and Druffel E. R. M. (2003) Organic and black carbon ^{13}C and ^{14}C through the Santa Monica Basin sediment oxic–anoxic transition. *Geophys. Res. Lett.* **30**. http://dx.doi.org/10.1029/2002GL015050.

Mayorga E., Aufdenkampe A. K., Masiello C. A., Krusche A. V., Hedges J. I., Quay P. D., Richey J. E. and Brown T. A. (2005) Young organic matter as a source of carbon dioxide outgassing from Amazonian rivers. *Nature* **436**, 538–541.

McCorkle D. C., Emerson S. and Quay P. D. (1985) Stable carbon isotopes in marine pore waters. *Earth Planet. Sci. Lett.* **74**, 13–26.

McManus J., Berelson W. M., Severman S., Poulson R. L., Hammond D. E., Klinkhammer G. P. and Holm C. (2006) Molybdenum and uranium geochemistry in continental margin sediments: paleoproxy potential. *Geochim. Cosmochim. Acta* **70**, 4643–4662.

McNichol A. P. and Aluwihare L. I. (2007) The power of radiocarbon in biogeochemical studies of the marine carbon cycle: insights from studies of dissolved and particulate organic carbon (DOC and POC). *Chem. Rev.* **107**, 443–466.

McNichol A. P., Jones G. A., Hutton D. L., Gagnon A. R. and Key R. M. (1994) The rapid preparation of seawater total CO_2 for radiocarbon analysis at the National Ocean Sciences AMS Facility. *Radiocarbon* **36**, 237–246.

Meysman F. J. R., Boudreau B. P. and Middelburg J. J. (2005) Modelling reactive transport in sediments subject to bioturbation and compaction. *Geochim. Cosmochim. Acta* **69**, 3601–3617.

Middelburg J. J. (1989) A simple rate model for organic matter decomposition in marine sediments. *Geochim. Cosmochim. Acta* **53**, 1577–1581.

Mollenhauer G. and Eglinton T. I. (2007) Diagenetic and sedimentological controls on the composition of organic matter preserved in California Borderland Basin sediments. *Limnol. Oceanogr.* **52**, 558–576.

Mook W. G. and van der Plicht H. (1999) Reporting ^{14}C activities and concentrations. *Radiocarbon* **41**, 227–239.

Mopper K. and Kieber D. J. (2002) Photochemistry and the cycling of carbon, sulfur, nitrogen and phosphorus. In *Biogeochemistry of Marine Dissolved Organic Matter* (eds. D. A. Hansell and C. A. Carlson). Academic Press.

Pearson A. and Eglinton T. I. (2000) The origin of *n*-alkanes in Santa Monica Basin surface sediment: a model based on compound-specific $\Delta^{14}C$ and $\delta^{13}C$ data. *Org. Geochem.* **31**, 1103–1116.

Pearson A., Eglinton L. and McNichol A. P. (2000) An organic tracer for surface ocean radiocarbon. *Paleoceanography* **15**, 541–550.

Pearson A., McNichol A. P., Benitez-Nelson B. C., Hayes J. M. and Eglinton T. I. (2001) Origins of lipid biomarkers in Santa Monica Basin surface sediment: a case study using compound-specific $\Delta^{14}C$ analysis. *Geochim. Cosmochim. Acta* **65**, 3123–3137.

Penning H. and Conrad R. (2006) Carbon isotope effects associated with mixed-acid fermentation of saccharides by *Clostridium papyrosolvens*. *Geochim. Cosmochim. Acta* **70**, 2283–2297.

Prokopenko M., Sigman D. M., Berelson W. M., Hammond D. E., Barnett B., Chong L. S. and Townsend-Small A. (2011) Denitrification in anoxic sediments supported by biological nitrate transport. *Geochim. Cosmochim. Acta* **75**, 7180–7199.

Purinton B. L., DeMaster D. J., Thomas C. J. and Smith C. R. (2008) ^{14}C as tracer of labile organic matter in Antarctic benthic food webs. *Deep Sea Res. Part II* **55**, 2438–2450.

Repeta D. J. and Aluwihare L. I. (2006) Radiocarbon analysis of neutral sugars in high-molecular-weight dissolved organic carbon: implications for organic carbon cycling. *Limnol. Oceanogr.* **51**, 1045–1053.

Robador A., Bruchert V., Steen A. D. and Arnosti C. (2010) Temperature induced decoupling of enzymatic hydrolysis and carbon remineralization in long-term incubations of Arctic and temperate sediments. *Geochim. Cosmochim. Acta* **74**, 2316–2326.

Romans B. W., Normark W. R., McGann M. M., Covault J. A. and Graham S. A. (2009) Coarse-grained sediment delivery and distribution in the Holocene Santa Monica Basin, California: implications for evaluating source-to-sink flux at millenial time scales. *Geol. Soc. Am. Bull.* **121**(9/10), 1392–1408.

Sansone F. J. and Martens C. S. (1982) Volatile fatty acid cycling in organic-rich marine sediments. *Geochim. Cosmochim. Acta* **46**, 1575–1589.

Schmidt F., Koch B. P., Elvert M., Schmidt G., Witt M. and Hinrichs K.-U. (2011) Diagenetic transformation of dissolved organic nitrogen compounds under contrasting sedimentary redox conditions in the Black Sea. *Environ. Sci. Technol.* **45**, 5223–5229.

Schulz H. D. (2006) Quantification of early diagenesis: dissolved constituents in marine pore water. In *Marine Geochemistry* (eds. H. D. Schulz and M. Zabel). Springer.

Shah S. R., Mollenhauer G., Ohkouchi N., Eglinton T. I. and Pearson A. (2008) Origins of archaeal tetraether lipids in sediments: insights from radiocarbon analysis. *Geochim. Cosmochim. Acta* **72**, 4577–4594.

Stuiver M. and Polach H. A. (1977) Reporting of ^{14} C data. *Radiocarbon* **19**, 355–363.

Tremblay L. B., Dittmar T., Marshall A. G., Cooper W. J. and Cooper W. T. (2007) Molecular characterization of dissolved organic matter in a North Brazilian mangrove porewater and mangrove-fringed estuaries by ultrahigh resolution Fourier transform-ion cyclotron resonance mass spectrometry and excitation/emission spectroscopy. *Mar. Chem.* **105**, 15–29.

Trumbore S. (2000) Age of soil organic matter and soil respiration: radiocarbon constraints on belowground C dynamics. *Ecol. Appl.* **10**, 399–411.

Tupas L. M., Popp B. N. and Karl D. M. (1994) Dissolved organic carbon in oligotrophic waters: experiments on sample preservation, storage and analysis. *Mar. Chem.* **45**, 207–216.

Waltz P. M. and Friederich G. E. (1996) Rapid automated analysis of total dissolved inorganic carbon and its application in the central California upwelling system during the CoOP95 experiment. *EOS* **76**, OS102.

Wang X.-C., Druffel E. R. M., Griffin S., Lee C. and Kashgarian M. (1998) Radiocarbon studies of organic compound classes in plankton and sediment of the northeastern Pacific Ocean. *Geochim. Cosmochim. Acta* **62**, 1365–1378.

Westrich J. T. and Berner R. A. (1984) The role of sedimentary organic matter in bacterial sulfate reduction: the *G* model tested. *Limnol. Oceanogr.* **29**, 236–249.

Williams P. M., Robertson K. J., Soutar A., Griffin S. M. and Druffel E. R. M. (1992) Isotopic signatures (^{13}C, ^{14}C, ^{15}N) as tracers of sources and cycling of soluble and particulate organic matter in the Santa Monica Basin, California. *Prog. Oceanogr.* **30**, 253–290.

Xu X., Zheng S., Southon J. R., McDuffee K. E., Luttgen M. and Liu J. C. (2007) Modifying a sealed tube zinc reduction method for preparation of AMS graphite targets: reducing background and attaining high precision. *Nucl. Instr. Meth. Phys. Res. B* **259**, 320–329.

Associate editor: James McManus